



Published in final edited form as:

*Dev Cell.* 2021 May 17; 56(10): 1484–1497.e7. doi:10.1016/j.devcel.2021.03.031.

## A G protein-coupled receptor-like module regulates cellulose synthase secretion from the endomembrane system in *Arabidopsis*

Heather E. McFarlane<sup>1,2,3,\*</sup>, Daniela Mutwil-Anderwald<sup>2,4</sup>, Jana Verban i<sup>1,2</sup>, Kelsey L. Picard<sup>1,5</sup>, Timothy E. Gookin<sup>6</sup>, Anja Froehlich<sup>2</sup>, David Chakravorty<sup>6</sup>, Luisa M. Trindade<sup>7</sup>, Jose M. Alonso<sup>8</sup>, Sarah M. Assmann<sup>6</sup>, Staffan Persson<sup>1,2,9,10,11,12,\*</sup>

<sup>1</sup>School of Biosciences, University of Melbourne, Parkville 3010 VIC, Australia

<sup>2</sup>Max-Planck Institute for Molecular Plant Physiology, Am Muehlenberg 1, 14476 Potsdam, Germany

<sup>3</sup>Department of Cell and Systems Biology, University of Toronto, 25 Harbord St, Toronto, ON M5S 3G5, Canada

<sup>4</sup>School of the Biological Sciences, Nanyang Technological University, 60 Nanyang Drive, Singapore 637551, Singapore

<sup>5</sup>School of Natural Sciences, University of Tasmania, Hobart 7001 TAS, Australia

<sup>6</sup>Department of Biology, The Pennsylvania State University, Mueller Laboratory, University Park, PA 16802, USA

<sup>7</sup>Plant Breeding, Wageningen University and Research, Droevendaalsesteeg 1, 6708 PB Wageningen, the Netherlands

<sup>8</sup>Department of Plant and Microbial Biology, Program in Genetics, North Carolina State University, Raleigh, NC 27695-7614, USA

<sup>9</sup>Department of Plant & Environmental Sciences, University of Copenhagen, 1871 Frederiksberg C, Denmark

<sup>10</sup>Copenhagen Plant Science Center, University of Copenhagen, 1871 Frederiksberg C, Denmark

<sup>11</sup>Joint International Research Laboratory of Metabolic & Developmental Sciences, State Key Laboratory of Hybrid Rice, SJTU-University of Adelaide Joint Centre for Agriculture and Health, School of Life Sciences and Biotechnology, Shanghai Jiao Tong University, Shanghai, China

<sup>12</sup>Lead contact

\*Correspondence: h.mcfarlane@utoronto.ca (H.E.M.), staffan.persson@plen.ku.dk (S.P).

#### AUTHOR CONTRIBUTIONS

Conceptualization, H.E.M., D.M.-A., S.M.A., and S.P.; investigation, H.E.M., D.M.-A., J.V., K.L.P., T.E.G., A.F., D.C., and S.P.; resources, J.M.A.; writing – original draft, H.E.M. and S.P.; writing – reviewing & editing, H.E.M., T.E.G., D.C., S.M.A., and S.P.; supervision, H.E.M., S.M.A., and S.P.; funding acquisition, H.E.M., S.M.A., and S.P.

#### DECLARATION OF INTERESTS

The authors declare no competing interests.

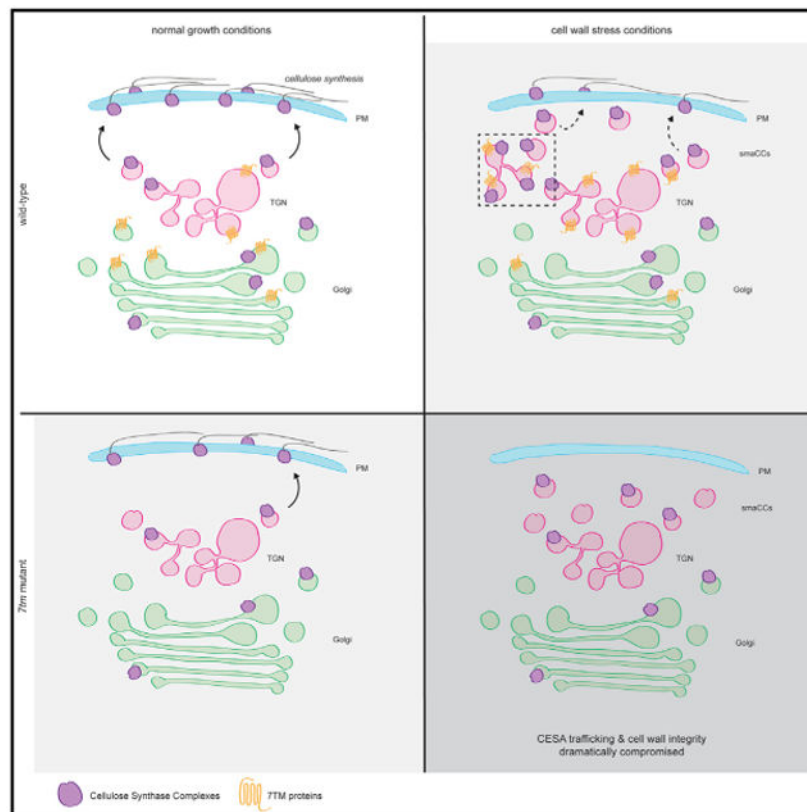
#### SUPPLEMENTAL INFORMATION

Supplemental information can be found online at <https://doi.org/10.1016/j.devcel.2021.03.031>.

## SUMMARY

Cellulose is produced at the plasma membrane of plant cells by cellulose synthase (CESA) complexes (CSCs). CSCs are assembled in the endomembrane system and then trafficked to the plasma membrane. Because CESAs are only active in the plasma membrane, control of CSC secretion regulates cellulose synthesis. We identified members of a family of seven transmembrane domain-containing proteins (7TMs) that are important for cellulose production during cell wall integrity stress. 7TMs are often associated with guanine nucleotide-binding (G) protein signaling and we found that mutants affecting the G $\beta\gamma$  dimer phenocopied the *7tm* mutants. Unexpectedly, the 7TMs localized to the Golgi/*trans*-Golgi network where they interacted with G protein components. Here, the 7TMs and G $\beta\gamma$  regulated CESA trafficking but did not affect general protein secretion. Our results outline how a G protein-coupled module regulates CESA trafficking and reveal that defects in this process lead to exacerbated responses to cell wall integrity stress.

## Graphical abstract



## In brief

The cell wall provides mechanical support and protection to plant cells. McFarlane et al. characterize a mechanism by which plants fortify their cell walls under stress through the action of a G protein-coupled receptor-like module that facilitates secretion of cell wall synthesis enzymes.

## INTRODUCTION

The plant primary cell wall is a polysaccharide-based cellular exoskeleton that provides the basis for directed plant growth and protects the cell. Cellulose, the main component of primary cell walls, consists of  $\beta$ -1,4-linked glucans that coalesce into microfibrils through hydrogen bonding (Anderson and Kieber, 2020). These microfibrils are the load-bearing structures of growing plant cell walls and their abundance and orientation therefore dictate the mechanical properties of most cell walls. Cellulose is synthesized by cellulose synthase (CESA) complexes (CSCs) at the plasma membrane. CSCs consist of three structurally related CESA subunits. In *Arabidopsis thaliana*, CESA1, 3, and 6-like CESAs contribute to synthesis of the primary walls that surround all plant cells (Desprez et al., 2007; Persson et al., 2007).

Because CESA enzymes are only active in the plasma membrane, control of CSC secretion and endocytosis is a critical step in regulating cellulose synthesis (McFarlane et al., 2014). Several factors contribute to CSC secretion, including the actin cytoskeleton (Sampathkumar et al., 2013; Zhang et al., 2019), PATROL1 via the exocyst complex (Zhu et al., 2018), SHOU4 (Polko et al., 2018), and the kinesin FRA1 (Zhu et al., 2015). In addition, two proteins, STELLO (STL) 1 and 2, regulate CSC secretion from the Golgi, perhaps by aiding in the assembly of the CSC (Zhang et al., 2016). Several small molecules also affect CSC trafficking (DeBolt et al., 2007; Worden et al., 2015). For example, isoxaben causes rapid internalization of CSCs into small CESA-containing compartments (SmaCCs; Gutierrez et al., 2009; Crowell et al., 2009). Once in the plasma membrane, CSCs are activated and laterally diffuse in the membrane to synthesize cellulose (Paredez et al., 2006). The direction of CSC movement can be steered by cortical microtubules (Paredez et al., 2006; Chan and Coen, 2020). Eventually, CSCs stall and are internalized into the cell via clathrin-mediated endocytosis (Sánchez-Rodríguez et al., 2018).

Plant cell walls are dynamic structures that undergo changes in response to environmental and developmental signals. Similar to yeast, plant cells utilize mechanisms to perceive and respond to changes in cell wall integrity (CWI) (Vaahtera et al., 2019; Rui and Dinneny, 2020). CWI changes can be induced by short-term cell wall inhibitor treatments (e.g., with the cellulose synthesis inhibitor, isoxaben) or via chronic alterations to cell wall synthesis or remodeling (Denness et al., 2011). Isoxaben is a particularly powerful tool for studying CWI as it seems to directly target cellulose synthesis. Screens for isoxaben resistance have revealed that point mutations in CESA3 and CESA6 confer increased tolerance to isoxaben (Shim et al., 2018), which indicates that isoxaben triggers CWI signaling by reducing cellulose synthesis, presumably through direct inhibition of CESA enzymes.

Because CWI is likely sensed at the interface between the cell wall and the plasma membrane, the search for components that monitor CWI has largely focused on plasma membrane-localized proteins. Several receptor-like kinases (RLKs) have been implicated in CWI sensing, including members of the *Catharanthus roseus* RLK-like family, or CrRLKs (Hématy et al., 2007; Haruta et al., 2014; Gonneau et al., 2018; Feng et al., 2018) and wall-associated kinases (WAKs) (Kohorn and Kohorn, 2012). The heterotrimeric guanine nucleotide-binding (G) protein complex has also been linked to CWI signaling (Klopffleisch

et al., 2011; Delgado-Cerezo et al., 2012). This complex, composed of  $G\alpha$ ,  $G\beta$ , and  $G\gamma$  subunits, is conserved across eukaryotes, although there are substantial differences in number of genes encoding these subunits and their activities in plants and animals (Maruta et al., 2019). In the textbook model of G protein signaling, a plasma membrane-localized G protein-coupled receptor (GPCR) with seven transmembrane domains perceives an extracellular signal, resulting in  $G\alpha$  exchange of GDP for GTP. This exchange results in the dissociation of the  $G\alpha\beta\gamma$  heterotrimer so that GTP-bound  $G\alpha$  and the  $G\beta\gamma$  dimer can elicit different intracellular signaling responses (Pandey, 2019). In the context of CWI signaling, components of the G protein signaling pathway have been linked to cell proliferation and cell expansion in plants (Ullah et al., 2001; Ullah et al., 2003; Chen et al., 2003; Jaffé et al., 2012; Roy Choudhury et al., 2019), and also to pathogen-associated molecular pattern (PAMP)-triggered immunity (Sánchez-Rodríguez et al., 2009; Aranda-Sicilia et al., 2015; Tunc-Ozdemir et al., 2016; Liang et al., 2016; Escudero et al., 2017), all of which require close communication between the plant cell and its cell wall. A predicted interactome of G protein components in Arabidopsis revealed links to cell wall synthesis and modification proteins and several canonical G protein complex mutants had altered cell wall composition (Kloppfleisch et al., 2011). Similarly, Delgado-Cerezo et al. (2012) demonstrated that transcriptomic changes in  $G\beta$  and  $G\gamma$  mutants are similar and enriched in cell wall synthesis and modification genes. Together, these studies make components of the G protein complex, and their putative receptors, exciting candidates for CWI signaling components.

## RESULTS

### Seven transmembrane proteins are required for seedling growth during cell wall stress

Cellulose synthesis-associated genes tend to be co-expressed with the *CESA* genes (Persson et al., 2005). We employed the tool FamNet (Ruprecht et al., 2016) to identify genes and gene families (pfams) that are co-expressed with the primary wall *CESAs* across many tissues and conditions (Figures S1A and S1B). We obtained T-DNA lines that disrupted several of the co-expressed genes and grew seedlings on control media, or media supplemented with isoxaben, a potent and specific cellulose synthesis inhibitor that directly affects CESA activity (Heim et al., 1990; Shim et al., 2018). Two T-DNA lines that targeted At5g18520, which corresponds to a putative seven transmembrane domain (7TM)-containing protein, displayed reduced root and hypocotyl lengths, thicker hypocotyls on isoxaben-supplemented media and reduced transcript levels (*7tm1-1*) or no detectable transcript (*7tm1-2*) for the gene (Figures 1A-1D and S2A). The mutants did not show any phenotypic deviations from wild type on media without isoxaben or under unstressed growth conditions (Figure S2).

*7TM* is part of a small gene family in Arabidopsis (Figure S2B) and therefore we refer to At5g18520 as *7TM1*. We isolated T-DNA insertion mutants for each of the other members of the *7TM* clade, i.e., *7TM2* (At3g09570), *7TM3* (At5g02630), and *7TM4* (At5g42090). We also included *7TM5* (At2g01070), which is in a second clade of *7TM*s, as this gene was highly co-expressed with *7TM1* (Table S1). Of these mutants, only the *7tm1* single mutant seedlings displayed increased sensitivity to isoxaben compared with the wild type (Figure S2C). Because all five *7TM* genes are expressed throughout plant growth and development

(Figures S1C-S1F; Waese et al., 2017), we generated double mutant combinations between *7tm1-2* and the other *7tm* mutants to assess potential functional redundancy among the 7TM family. Of the combinations we assayed, only *7tm1 7tm5* double mutant seedlings displayed enhanced isoxaben sensitivity compared with *7tm1* seedlings (Figures 1A-1D and S2C). The *7tm1* and *7tm1-2 7tm5-1* mutants also displayed increased sensitivity to the cellulose synthesis inhibitor 2,6-dichlorobenzonitrile (DCB; Figures 1E and S3). Although cellulose synthesis inhibitors decreased hypocotyl length of *7tm1* seedlings relative to wild type, other inhibitors or stress conditions, including high sucrose, salinity, oryzalin, latrunculin B, concanamycin A, or wortmannin, did not significantly affect hypocotyl length of *7tm* mutants relative to wild type (Figure S3).

Cryo-scanning electron microscopy of etiolated seedlings grown on isoxaben-containing media revealed that the increased *7tm1* and *7tm1 7tm5* hypocotyl thickness was primarily caused by epidermal cell swelling (Figures 1F and 1G), which is a common phenotype of cellulose synthesis deficiency (e.g., Arioli et al., 1998; Desprez et al., 2007; Persson et al., 2007). To further assess its role in cellulose synthesis, we introgressed *7tm1-2* into *procuste1-1 (prc1-1)*, a null mutation in *CESA6* (Fagard et al., 2000). The double homozygous progeny of *7tm1-2 prc1-1* displayed slightly decreased hypocotyl length compared with the parent lines (Figure S4A), although this was not statistically significant owing to the already strong effects of the *prc1-1* mutation on hypocotyl elongation (Fagard et al., 2000).

To assess whether the mutant seedlings were affected in their ability to produce cellulose, we measured cellulose content in etiolated 7-day-old wild type, *7tm1*, and *7tm1 7tm5* seedlings. Under normal growth conditions, there was no significant difference in the level of cellulose between *7tm* mutants and wild type (Figure 1H). However, when grown on isoxaben, the *7tm1 7tm5* mutants had significantly less cellulose than wild-type seedlings (Figure 1H).

### Components of the G protein signaling complex are required for seedling growth during cell wall stress

The 7TM family has previously been annotated as putative GPCRs based on *in silico* predictions and protein-protein interaction assays (Gookin et al., 2008). This suggested that components of the G protein signaling pathway may also be required for seedling growth under cell wall stress. Therefore, we assayed the growth of mutants affecting the canonical heterotrimeric G protein signaling components, including G $\alpha$  (GPA1), G $\beta$  (AGB1), and G $\gamma$  (AGG1, AGG2, and AGG3) (Ullah et al., 2003; Trusov et al., 2007; Fan et al., 2008; Chakravorty et al., 2011) on media containing isoxaben and other stress conditions (Figures 2, S2, and S3). Similar to the *7tm1* and *7tm1 7tm5* mutants, single knockout mutants for the sole canonical G $\beta$  subunit (*agb1-2*) and a triple mutant for all three G $\gamma$  subunits (*agg1-1c agg2-1 agg3-1*) displayed reduced hypocotyl and root length and abnormal epidermal cell swelling when grown on isoxaben- and DCB-containing media (Figures 2A-2F and S3). Furthermore, the *agb1-2* single mutants and *agg1-1c agg2-1 agg3-1* triple mutants displayed a similar reduction in cellulose as the *7tm1* and *7tm1 7tm5* mutant seedlings when grown on isoxaben (Figure 2G).

To investigate whether the 7TMs and the G proteins work in a common genetic pathway, we produced *7tm1 7tm5 gpa1-4* and *7tm1 7tm5 agb1-2* triple mutants and assessed seedling length on isoxaben-containing media. Consistent with their action in a linear pathway, triple mutant seedlings displayed similar phenotypes to that of the most severely affected parental lines (Figures 3A and S4B).

Canonical GPCRs interact with the G protein complex via the G $\alpha$  subunit (Pandey, 2019) and 7TM1 was previously shown to physically interact with the G $\alpha$  subunit in a yeast split-ubiquitin interaction system (Gookin et al., 2008). To corroborate these results, we used a modified bimolecular fluorescence complementation (BiFC) system in which both genes of interest are on the same binary vector, which negates issues of different transformation efficiencies and expression levels of the two candidate interactors (Gookin and Assmann, 2014). We observed clear fluorescent signal when a vector containing both 7TM1-cYFP and G $\alpha$ -nYFP, or both 7TM5-cYFP and G $\alpha$ -nYFP, was transformed into *N. benthamiana* leaves (Figures 3B and S4C). Surprisingly, the BiFC signals between 7TMs and G $\alpha$  were associated with intracellular puncta. When this BiFC vector was co-transformed with a Golgi marker (RFP-XYLT; Saint-Jore-Dupas et al., 2006), there was substantial colocalization between YFP and RFP (Figures 3B and S4C). As a control, we used the modified BiFC system to transform a vector containing 7TM1-nYFP and PIP2A-cYFP or 7TM5-nYFP and PIP2A-cYFP because PIP2A is a plasma membrane-localized protein with a similar localization to previous reports of G $\alpha$  (Chen et al., 2003) and included a Golgi marker (mTurquoise-XYLT; Saint-Jore-Dupas et al., 2006) on the same vector backbone as a positive control for transformation. In this case, we did not detect any YFP BiFC signal in cells that expressed the Golgi marker (Figure S4C). We also tested for non-canonical interactions between the 7TMs and the G protein complex via G $\beta$ . No substantial interaction was detected between 7TM1-cYFP and G $\beta$ -nYFP or 7TM5-cYFP and G $\beta$ -nYFP, whether in the presence or absence of any of the G $\gamma$  subunits (Figure S4C). We occasionally observed a very weak signal generated from 7TM1-G $\beta$  in the presence of AGG2, but the signal was infrequently observed and substantially weaker than the positive control. Taken together, the common phenotypes, genetic interactions, split-ubiquitin (Gookin et al., 2008), and BiFC data support that 7TM1 and 7TM5 can interact with the G protein complex through G $\alpha$  and that normal functions of the G $\beta$  and G $\gamma$  subunits are crucial for tolerance to CWI stress. These results imply that 7TM1 and 7TM5 can interact with the G protein complex in a similar fashion to canonical GPCRs and that the phenotypes assayed here are dependent upon the G $\beta\gamma$  dimer.

### A sub-population of G protein components associates with the Golgi apparatus and TGN

We next investigated the subcellular localization of G protein components. G protein localization data in plants are largely based on constitutive promoter-driven constructs in heterologous systems (Chen et al., 2003; Anderson and Botella, 2007; Zeng et al., 2007), which are prone to localization artifacts. Therefore, we generated native promoter-driven fluorescent protein fusions for G $\alpha$ , G $\beta$  and all three G $\gamma$  subunits and transformed these into their corresponding knockout mutants. Because no signal was detected from native promoter-driven G $\alpha$  fluorescent protein fusions, we also constructed *Ubiquitin10* promoter-driven GFP fusions for G $\alpha$ . The *Ubiquitin10* promoter-driven G $\alpha$ -GFP and GFP-G $\alpha$  and the

native promoter-driven genomic G $\beta$ -mCherry and mCherry-G $\gamma$  constructs partially or fully complemented the respective mutant phenotypes (Figure S5A). For all lines, we detected stable fluorescent protein signal at the plasma membrane of young root epidermal cells, where signals were strongest (Figure S5B). We also detected some intracellular signals in several of the lines; however, this was difficult to visualize owing to low fluorescence. Therefore, we treated these lines with Brefeldin A (BFA), a fungal toxin that causes aggregation of the TGN and post-Golgi compartments in *Arabidopsis* root cells into a “BFA body,” and clustering of intact Golgi stacks around the BFA body (Richter et al., 2007). BFA treatment resulted in signal aggregation of GFP-G $\alpha$ , G $\alpha$ -GFP, and G $\beta$ -mCherry in intracellular BFA bodies (Figure S5B), indicating that these proteins can at least partially associate with the TGN or post-Golgi compartments. By contrast, we could not detect signal from the fluorescently tagged G $\gamma$  subunits at BFA bodies (Figure S5B). Given that a G $\beta$  subunit and a G $\gamma$  subunit typically signal together (Pandey, 2019), the absence of a clear fluorescent signal of the mCherry-AGG1, mCherry-AGG2, or mCherry-AGG3 fusions within the endomembrane system could indicate that the tag may interfere with some, but not all, of the AGG functions, or that the endomembrane signal is too dim to reliably detect.

### 7TM1 and 7TM5 act at the Golgi apparatus and *trans*-Golgi network

The punctate BiFC signal from the interaction between 7TM1/7TM5 and GPA1 indicated that the 7TMs may be localized to the endomembrane system. To test this, we generated a native promoter-driven genomic triple-YFP fusion to 7TM1 (7TM1-3xYFP) via recombineering (Brumos et al., 2020) and transformed the construct into *7tm1-2* mutant plants. This construct restored the length of *7tm1-2* mutant seedlings on isoxaben to nearly wild-type levels (Figure S6A), indicating that the 7TM1-3xYFP fusion was functional. We also generated a functional 7TM5-CFP fusion, driven by a 35S-promoter, and another native promoter-driven genomic 7TM1-mCherry construct via recombineering, for colocalization purposes. Time-lapse imaging in etiolated hypocotyl cells revealed that 7TM1-3xYFP, 7TM1-mCherry, and 7TM5-CFP were localized to intracellular puncta that rapidly streamed in the cytoplasm (Figure 4A; Video S1).

To confirm 7TM1 and 7TM5 localization to the Golgi apparatus and TGN, we crossed the 7TM1-3xYFP, 7TM1-mCherry, and 7TM5-CFP lines to markers for different endomembrane compartments, including the Golgi apparatus (YFP-CESA6 and WAVE18-RFP), the TGN (WAVE13-RFP and VHAa1-mRFP), and the late endosome (WAVE2-RFP and WAVE7-RFP) (Paredes et al., 2006; Dettmer et al., 2006; Geldner et al., 2009). Object-based colocalization (Bolte and Cordelières, 2006) was equally high between 7TM1 and 7TM5 with markers for both the Golgi apparatus and the TGN (Figures 4B, 4C, and S6B), indicating that the steady-state localizations of the 7TM1 and 7TM5 protein fusions are at the Golgi and TGN. These results are consistent with several proteomic studies that have detected 7TM1 and 7TM5 in Golgi or TGN-associated proteomes (Dunkley et al., 2006; Parsons et al., 2012; Groen et al., 2014).

## Overall structure and function of the Golgi apparatus and TGN are not affected in *7tm1 7tm5* and *agb1* mutants

The localization of 7TM1 and 7TM5 to the Golgi and TGN implies that they may play a role in Golgi or TGN function. To assess this, we first crossed the Golgi marker, NAG-GFP (Grebe et al., 2003) into the *7tm1 7tm5* double mutants. We found no significant differences in NAG-GFP distribution or dynamics in live etiolated hypocotyl cells of *7tm1 7tm5* mutants compared with wild type (Figure 5A; Video S2). Neither short-term (200 nM for 2 h) nor long-term (2 nM for 3 days) isoxaben treatment caused any major alterations to the distribution or behavior of NAG-GFP in the *7tm1 7tm5* mutants etiolated hypocotyl cells relative to wild type (Figure 5A).

We next examined the ultrastructure of the secretory pathway in high-pressure frozen, freeze-substituted etiolated hypocotyl cells. The structures of the Golgi apparatus and TGN were comparable between wild type, *agb1-2* and *7tm1 7tm5* mutants (Figures 5B and S7A). Neither short-term (200 nM for 2 h) nor long-term (2 nM for 3 days) isoxaben treatment caused any substantial defects to Golgi or TGN structure in etiolated hypocotyl cells of the *7tm1 7tm5* or *agb1-2* mutants, relative to wild type (Figures 5B and S7A). These results indicate that there are no large-scale defects in Golgi or TGN structure or function owing to loss of 7TM1 and 7TM5 or the G protein complex (via AGB1).

To determine whether secretion of plasma membrane protein cargo was affected in the *7tm1 7tm5* and *agb1-2* mutants, we crossed lines expressing the fluorescent plasma membrane protein GFP-LTI6b (Cutler et al., 2000) into the mutant plants. We found that the steady-state localization of GFP-LTI6b was similar in etiolated hypocotyls of *7tm1 7tm5*, *agb1-2*, and wild-type plants, and that this localization was unaffected by short-term isoxaben treatment (Figures 5C, 5D, and S7B). To determine whether soluble protein secretion was affected, we crossed a ratiometric-based sec-GFP (versus endomembrane-targeted RFP; Samalova et al., 2006) into the *7tm1 7tm5* and *agb1-2* mutants. Sec-GFP is a modified GFP with a signal peptide that directs the protein to the secretory pathway and ultimately to the apoplast, where the GFP fluorescence is quenched by the low pH. We found no significant difference in the ratiometric sec-GFP marker between *7tm1 7tm5*, *agb1-2*, and wild-type plants, indicating that secretion of this soluble protein is unaffected in the mutants (Figures 5E and S7C).

Because the plant TGN also acts as an early endosome (Dettmer et al., 2006), we evaluated endocytic trafficking to the TGN by tracking uptake of the fluorescent membrane dye, FM4-64, in seedling roots. FM4-64 initially labels the plasma membrane, then travels to the early endosome/TGN, late endosome and finally the tonoplast (vacuole membrane) over ~3 h. There were no significant differences in either the rate of uptake of FM4-64 or the number of fluorescent puncta at various time points between wild type and either *7tm1 7tm5* or *agb1-2* mutants (Figures 5F, 5G, and S7D).

In summary, despite the Golgi and TGN localization of the 7TM1 and 7TM5, it does not seem that loss of these proteins has any substantial consequences for the structures or functions of the Golgi apparatus or TGN. These data are consistent with the mostly normal overall growth of *agb1-2* and *7tm1 7tm5* plants under standard growth conditions (Figures

S2D and S2E), as mutant plants with dramatic Golgi/TGN morphology or secretion defects are usually dwarf, bushy, semi-sterile and exhibit other pleiotropic phenotypes (e.g., Teh and Moore, 2007; Richter et al., 2007; Gendre et al., 2013).

### **CSC trafficking is defective in *7tm1 7tm5* and *agb1* mutants**

To gain further mechanistic insight into the cellulose defect in *7tm1 7tm5* and G protein mutants *gpa1-4* and *agb1-2*, we crossed them with the CESA marker lines YFP-CESA6 (Paredes et al., 2006) or GFP-CESA3 (Desprez et al., 2007) to monitor the behavior of primary cell wall CSCs. The rate of cellulose synthesis is thought to correspond to the speed of fluorescent CESA puncta movement in the plasma membrane (Paredes et al., 2006). Consistent with our cellulose assays, we did not detect any significant differences in YFP-CESA6 puncta speed at the plasma membrane in the *7tm1 7tm5*, *agb1-2*, or *gpa1-4* mutants compared with wild type under control conditions (Figures 6A and S8A; Video S3). Similarly, we did not observe any differences in steady-state CSC density at the plasma membrane or in SmaCC density in the cortical cytoplasm between wild type and *7tm1 7tm5* mutants under control conditions (Figures 6B and S8A).

Because 7TM1-3xYFP and 7TM5-CFP are localized to the Golgi/TGN, it seemed possible that the Golgi distribution or trafficking of CESAs may be affected in the mutants. To investigate this, we tracked delivery of GFP-CESA3 labeled CSCs from the Golgi apparatus to the plasma membrane using a modified fluorescence recovery after photobleaching (FRAP) approach (Sampathkumar et al., 2013). In wild-type etiolated hypocotyl cells, CSCs recovered to nearly normal density within 10 min postbleach (Figures 6C and S8B). By contrast, the recovery of CSC density took substantially longer in the *7tm1 7tm5* and *agb1-2* mutants (Figure 6D). Consequently, we found that the rate of CSC insertion into the plasma membrane was significantly lower in the *7tm1 7tm5* and *agb1-2* mutants, relative to wild-type or *gpa1-4* mutants (Figures 6D and S8B).

As short-term isoxaben treatment leads to substantial removal of CESAs from the plasma membrane (DeBolt et al., 2007), it was intractable to monitor CESA delivery to, and behavior at, the plasma membrane under these conditions. Therefore, we chose to assess CESA behavior in seedlings grown on media supplemented with low concentrations of isoxaben. Here, we found substantially fewer GFP-CESA3 labeled CSCs at the plasma membrane in *7tm1 7tm5* double mutants, relative to wild type (Figure 6B). These data suggest that the mutations in the 7TMs and AGB1 impair cellulose synthesis through decreased CSC secretion, which is exacerbated under conditions of CWI stress.

### **7TM1 localization is biased from Golgi/TGN to SmaCCs upon cell wall stress treatment**

Isoxaben induces CSC internalization and/or reduces CSC secretion, resulting in an increase in intracellular CESAs in SmaCCs (Gutierrez et al., 2009), which are involved in either secretion, recycling or degradation of the CESAs (Hoffmann et al., 2021). We reasoned that if the 7TMs are actively promoting CSC secretion to the plasma membrane, we may expect to see them colocalize at least in part with some of the isoxaben-induced SmaCCs. We therefore monitored dual-labeled YFP-CESA6 and 7TM1-mCherry hypocotyl cells before and after short-term isoxaben treatment. Under control conditions, the two

fluorescent proteins colocalized at the Golgi apparatus and TGN (Figures 4 and 7A) and very few SmaCCs were found in these cells (Figure 7A). After 1 h treatment with 100 nM isoxaben, we observed reduced colocalization between YFP-CESA6 and 7TM1-mCherry signals (Figures 7A and 7B; Video S4). This reduction was largely caused by a decrease in Golgi localization of the 7TM1-mCherry signal. However, some SmaCCs were labeled by both 7TM1-mCherry and YFP-CESA6, and time-lapse imaging revealed erratic movement of these dual-labeled particles, in agreement with previous reports of SmaCC behavior (Figure 7C; Video S4). Interestingly, whereas the highly motile SmaCCs contained both signals, the vast majority of SmaCCs that were stalled at the cell cortex no longer contained 7TM1-mCherry signal (Video S4). These stalled SmaCCs are hypothesized to be a final step before CSC insertion into the plasma membrane (Gutierrez et al., 2009; Crowell et al., 2009). Together with our observations that there are no overall changes to Golgi and TGN structure or function in the *7tm1 7tm5* mutants (Figure 5), these results imply that the 7TM proteins may change their localization upon CWI stress to promote early stages of CESA secretion, before CSC insertion into the plasma membrane.

## DISCUSSION

Cellulose is synthesized at the plasma membrane by CSCs, and CSC trafficking to and from the plasma membrane represents a critical step in the regulation of cellulose synthesis. By contrast to most plasma membrane-localized proteins, the CESAs display a complex localization pattern, including association with the plasma membrane, Golgi apparatus, SmaCCs, and clathrin-coated vesicles (Paredes et al., 2006; Crowell et al., 2009; Gutierrez et al., 2009; Sánchez-Rodríguez et al., 2018). This complexity has prompted research into the mechanisms that govern CSC localization and trafficking as an important component of understanding cell wall synthesis. We identified members of a putative GPCR-like protein family, the 7TMs, that are important for CSC secretion and for seedling growth during cell wall stress. Our data indicate that these proteins regulate CSC trafficking from the Golgi apparatus and TGN, and that this role becomes particularly important during cell wall stress (see Graphical Abstract). It further appears that the 7TM-mediated CWI responses primarily require the G $\beta\gamma$  dimer, which can dissociate from the activated GTP-bound G $\alpha$  subunit. The similar isoxaben-sensitive phenotypes between *7tm1 7tm5* and *agb1-2* single mutants or *agg1-1c agg2-1 agg3-1* triple mutants and the genetic interaction between *7tm1 7tm5* and *agb1-2* demonstrate the major role of the G $\beta\gamma$  dimer in CWI responses via the 7TMs.

Interestingly, the Golgi/TGN localization of 7TM1 and 7TM5 is reminiscent of an “orphan” family of GPCRs that localize to the Golgi/TGN in animal cells and that may not act as canonical GPCRs (Tafesse et al., 2014). Indeed, the 7TM family are phylogenetically and structurally most similar to these “orphan” GPCR family members (Munk et al., 2019; Figure S2B), which include the Golgi and TGN localized GPR107 (Tafesse et al., 2014). Although depletion of GPR107 in HeLa cells did not significantly alter Golgi structure or bulk anterograde trafficking (i.e., secretion), it did substantially affect retrograde trafficking (Tafesse et al., 2014). Disrupting GPR107 in mouse fibroblast cells resulted in defects in both endocytosis and re-secretion of a subset of cargoes (Zhou et al., 2014). Similarly, overexpression of other members of this “orphan” family, TMEM87A or 87B, was sufficient to rescue trafficking defects in Golgi-associated retrograde protein (GARP)

complex disrupted HEK293 cells. The authors reasoned that these Golgi localized human 7TM proteins therefore play a role in retrograde and anterograde trafficking from the Golgi (Hirata et al., 2015).

By contrast to GPR107 family members, 7TM1 and 7TM5 do not appear to generally affect Golgi/TGN to plasma membrane trafficking but rather control trafficking of the CESAs between these compartments. Because *7tm1 7tm5* mutants displayed reduced CSC secretion under normal growth conditions (Figure 6), we propose that the 7TMs are important components of a G protein-mediated mechanism that maintains CSC secretion to the plasma membrane. SmaCCs are rare under control conditions and are difficult to distinguish from the TGN because they show significant albeit incomplete overlap with TGN markers (Gutierrez et al., 2009; Crowell et al., 2009); however, SmaCCs are dramatically induced under stress including salt stress (Endler et al., 2015), osmotic stress (Gutierrez et al., 2009), and cell wall stress (via isoxaben treatment; Paredes et al., 2006). Interestingly, a sub-population of the isoxaben-induced SmaCCs contained both CESAs and 7TM1. We envision that the SmaCCs consist of a heterogenous population of compartments, which is consistent with observations that different subpopulations of SmaCCs colocalize with different TGN markers (Gutierrez et al., 2009). A progressive change in SmaCC content may represent a “maturation” of the SmaCCs from the TGN when preparing to deliver CESAs to the plasma membrane (Hoffmann et al., 2021). Consistent with this hypothesis, we found that many of the rapidly moving SmaCCs contained both 7TM1-mCherry and YFP-CESA6 signal, whereas stalled cortical SmaCCs, which are about to deliver their CSC cargo, only contained YFP-CESA6. It is plausible that the SmaCCs could form large vesicle “clusters” similar to secretory vesicle clusters (Toyooka et al., 2009) or TGN remnants (Stahelin and Kang, 2008), and may exchange proteins and other materials that could contribute to SmaCC maturation. Although the loss of the GPCR-like maintenance mechanism may not be detrimental to plant growth under optimal growth conditions (i.e., seedlings growing on media plates), once challenged with cell wall stress, *7tm1*, *7tm1 7tm5*, and several mutants affecting the G protein complex displayed reduced root and hypocotyl lengths (Figures 1 and 2). The sensitivity of the *7tm1 7tm5*, *agb1-2* and *agg* mutants to isoxaben and DCB, and their reduced capacity to synthesize cellulose under these conditions indicate that these components are important for modulating CSC secretion during CWI stress. These results imply that the wild-type role of the GPCR-like module is to regulate CSC secretion, and to contribute to cell wall fortification, especially under CWI stress conditions. Therefore, the 7TMs, as part of a potential G protein module, may contribute to maintaining CSC density at the plasma membrane during fluctuating environmental conditions.

Members of the *Catharanthus roseus* receptor-like kinase-like (CrRLKL) family are associated with CWI signaling (Rui and Dinneny, 2020) and RLK activity has been linked to G protein signaling in plants (e.g., Bommert et al., 2013; Aranda-Sicilia et al., 2015; Liang et al., 2016; Tunc-Ozdemir et al., 2016). The RLK FERONIA senses cell wall softening and can engage with cell wall pectins (Feng et al., 2018). FERONIA can interact with the G $\beta$  subunit, AGB1, to control stomatal movement (Yu et al., 2018), which is related to pectin status (Amsbury et al., 2016; Rui et al., 2017). Therefore, FERONIA and/or other similar CrRLKLs are likely to play important roles in the perception of CWI stress at the plasma membrane. The G protein complex may constitute a framework for integrating CWI

signals and responses; the G protein complex could potentially sense cell wall status via association with RLKs at the plasma membrane and regulate CSC secretion via the 7TMs at the endomembrane system.

In summary, we propose that the 7TMs are important components of plant responses to CWI stress, rather than part of the initial signal perception machinery. Indeed, *7tm1 7tm5* mutants are hypersensitive to cellulose-related defects (Figure 1), which stands in contrast to some other CWI signal perception mutants, such as *the1*, which are relatively insensitive to CWI stress (Hématy et al., 2007). In the future it will be interesting investigate the extent to which these 7TM-mediated responses interact with previously characterized CWI sensing pathways.

### Limitations of this study

Typical of canonical GPCRs (Baltoumas et al., 2013; Pandey, 2019), the 7TMs interact with the G $\alpha$  subunit of the G protein complex (Figure 3). However, *gpa1-4* mutants did not phenocopy the *7tm* mutants (Figure 2). It is possible that the 7TMs might also interact with extra-large GTP-binding proteins (XLGs), which are a plant-specific family of atypical G $\alpha$  subunits (Chakravorty et al., 2015). If the 7TMs act via the XLGs, rather than, or redundantly with, the canonical G $\alpha$ , this would explain the lack of an isoxaben-sensitive phenotype for the *gpa1-4* mutant.

## STAR ★ METHODS

### RESOURCE AVAILABILITY

**Lead contact**—Further information and requests for resources and reagents should be directed to and will be fulfilled by the lead contact, Staffan Persson (staffan.persson@plen.ku.dk).

**Materials availability**—Plasmids and plant lines generated in this study will be made available on request to the lead contact, Staffan Persson (staffan.persson@plen.ku.dk).

**Data and code availability**—No large datasets or new code were generated as part of this study.

### EXPERIMENTAL MODEL AND SUBJECT DETAILS

**Arabidopsis thaliana**—*Arabidopsis thaliana* seeds were surface sterilized and sown on ½ MS media (Duchefa) with 1% sucrose (Sigma; unless otherwise indicated, all chemicals were from Sigma) and 2.5 mM MES at pH 5.8, stratified for 2-3 days in the dark at 4°C, then moved to environmental growth chambers or growth rooms under long-day conditions: 18 h light at ~120  $\mu\text{mol m}^{-2} \text{s}^{-1}$  at 21°C and 6 h dark at 18°C. After 7-14 days, seedlings were transferred to soil and returned to the same conditions. For etiolated hypocotyl growth, seeds were exposed to white light (~120  $\mu\text{mol m}^{-2} \text{s}^{-1}$  21°C) for 3 hours, then plates were wrapped in foil and returned to the long-day growth conditions until required for experiments.

*7tm1-1* (SAIL\_701\_G12), *7tm1-2* (Salk\_134021) and *7tm5-1* (Salk\_044297) were obtained from the Arabidopsis Biological Resource Centre. Complete details of all mutants and marker lines are included in the STAR Methods Table. Plants were genotyped via PCR using primers indicated in Table S2.

**Nicotiana benthamiana**—For BiFC assays, *Nicotiana benthamiana* seeds were sown directly on soil and grown under the same conditions as Arabidopsis.

## METHOD DETAILS

**Plant growth assays**—For long-term inhibitor experiments, media was supplemented with 0.5-2 nM isoxaben from a 20 µM stock in ethanol, or 200 nM 2,6-Dichlorobenzonitrile (DCB) from a 20 µM stock in ethanol, as indicated. Plates were scanned using an Epson 1000XL flat-bed scanner and root or hypocotyl lengths were measured using a segmented line in Fiji. Individual hypocotyls were photographed using a Leica M205FA microscope with a DMC4500 camera.

**RT-PCR**—Seven-day-old light-grown seedlings were flash-frozen in liquid nitrogen and RNA was extracted using the Qiagen Plant RNeasy Mini kit according to the manufacturer's instructions. RNA integrity was verified via gel electrophoresis. DNA was removed by treatment with DnaseI (Amp-grade, Invitrogen) and cDNA was generated using the SSVI first strand synthesis kit (Invitrogen) with the oligo dT<sub>20</sub> primer provided, according to the manufacturer's instructions. RT-PCR was performed using primers indicated in Table S2.

**Cloning and plant transformation**—Fragments were amplified from genomic DNA (*7TM1*, *AGB1*, *AGG1*, *AGG2*, *AGG3*) or cDNA (*7TM5*, *GPA1*, *PIP2A*) using the primers indicated in Table S2.

Whole gene translational fusions between the *7TM1* and the reporters mCherry and 3xYPET were generated by recombineering as described in Brumos et al. (2020). Briefly, the JATY clone JATY76F23 carrying the *7TM1* gene was transferred to the *E. coli* recombineering strain SW105. The mCherry and 3xYPET cassettes were PCR amplified using the primers At5g18520CF and At5g18520CR, inserted in the *At5g18520* gene by recombineering to create in-frame C-terminus translational fusions and the recombinant products confirmed using the primers At5g18520CTF and At5g18520CTR. Finally, these DNA constructs were trimmed using the primers At5g18520delRB and At5g18520delLB and the deletions confirmed using the primers At5g18520delTRB and At5g18520delTLB. All primers are indicated in Table S2. Constructs were transformed into *7tm1-2* single mutants and *7tm1-2 7tm5-1* double mutants.

For *35S* promoter-driven *7TM5*-CFP, *7TM5* coding sequence was amplified without the stop codon using the primers indicated in Table S2 and transferred into the pEZR(K)-LNC binary vector via the EcoRI and BamHI sites. Constructs were transformed into *7tm5-1* single mutants and *7tm1-2 7tm5-1* double mutants.

For *Ubiquitin10* promoter-driven GFP-GPA1 and GPA1-GFP, *GPA1* coding sequence was amplified with or without the stop codon, respectively, from cDNA using the primers

indicated in Table S2 and transferred into pENTR-D-TOPO (Invitrogen) via Gibson assembly using NEB Gibson Assembly Master Mix according to the manufacturer's instructions. The GPA1 cassettes with and without the stop codon were then transferred to the pUBN-eGFP and pUBC-eGFP binary vectors (Grefen et al., 2010), respectively, via a Gateway LR reaction using LR Clonase II (Invitrogen) according to the manufacturer's instructions. Constructs were transformed into *gpa1-4* single mutants.

For native promoter-driven AGB1-mCherry, the *AGB1* genomic region from the start codon to immediately before the stop codon was inserted into pENTR-D-TOPO (Invitrogen) via TOPO cloning according to the manufacturer's instructions. Then the *AGB1* upstream regulatory region (~1.6 kb upstream of ATG, including the 5' UTR) was inserted into the NotI site of pENTR-D-TOPO and mCherry, including a stop codon, was inserted into the AscI site while also introducing a downstream KpnI site, and the downstream *AGB1* regulatory region (~400bp of 3' UTR) was inserted into this KpnI site.

For native promoter-driven mCherry-AGB1, the coding sequence of *mCherry* without a stop codon was inserted into pENTR-D-TOPO (Invitrogen) via TOPO cloning according to the manufacturer's instructions. Then, the upstream *AGB1* regulatory region (~1.6 kb upstream of ATG, including the 5' UTR) was inserted into the NotI site of pENTR-D-TOPO and the genomic sequence of AGB1 (from start codon to ~400bp downstream of the stop codon) was inserted into the AscI site.

For native promoter-driven mCherry-AGG1, mCherry-AGG2 and mCherry-AGG3, the same strategy was taken as for mCherry-AGB1; see Table S2 for primers. All of the *AGB1* and *AGG* cassettes were transferred to the pMDC99 binary vector (Curtis & Grossniklaus 2003) via a Gateway LR reaction using LR Clonase II (Invitrogen) according to the manufacturer's instructions. AGB constructs were transformed into *agb1-2* single mutants. AGG constructs were transformed into *agg1-1c agg2-1 agg3-1* triple mutants and the respective *agg* single mutants.

BiFC constructs were created in pDOE-05 with cDNA of *GPA1* or *AGB1* cloned into the NcoI-SpeI sites of MCS1 (nYFP fusion) with a complementary ligation of BspHI/NcoI overhangs at the 5' end of *AGB1*, as described in Gookin and Assmann (2014). *7TM1* or *7TM5* cDNAs were cloned into the KflI-AatII sites of MCS3 (cYFP fusion) with a complementary ligation of RsrII/KflI overhangs at the 5' ends of *7TM1* and *7TM5*. The *AGG1*, *AGG2* and *AGG3* expressing constructs were previously described in Gookin and Assmann (2014). *7TM/PIP2A* BiFC constructs were created in pDOE-10, with cDNA of *7TM1* or *7TM5* cDNAs cloned into MCS1 (nYFP fusion) and PIP2A cDNA cloned into MCS3 (cYFP fusion) using NEB Gibson Assembly Master Mix according to the manufacturer's instructions. Primers (Table S2) were designed to retain vector sequence either side of cDNA insertion into MCS.

For promoter:GUS fusions, *7TM1* and *7TM5*, promoter fragments of 1450 bp and 1700 bp, respectively, were amplified from Col-0 genomic DNA using the primers listed in Table S2 and ligated into pCAMBIA3201 (*7TM1*) and pCAMBIA1305.1 (*7TM5*) after restriction

enzyme digest with BamHI and NcoI. The verified constructs were transformed into Col-0. GUS staining was carried out according to Jefferson et al. (1987).

All constructs were verified via Sanger sequencing. Vectors were electroporated into *Agrobacterium tumefaciens* strain GV3101 and selected in half-salt LB media with appropriate antibiotics.

For stable Arabidopsis transformations, Agrobacteria from an overnight culture were harvested by centrifugation, then resuspended in a solution of 5% sucrose and 0.05% silwet L-77 (PhytoTech Labs). Young (~4 week-old) Arabidopsis plants were submerged in this solution for one minute, then returned to growth conditions. Seedlings were selected for positive transformants on 50 µg/mL kanamycin, 15 µg/mL glufosinate ammonium, or 30 µg/mL hygromycin, as appropriate. T3 lines that were likely homozygous for single insertions were selected based on segregation of the selection marker.

For BiFC, Agrobacteria from an overnight culture were harvested by centrifugation, then resuspended in a solution of 10 mM MES, 10 mM MgSO<sub>4</sub> and 75 µM acetosyringone (PhytoTech Labs) from a 100 mM stock in DMSO to a final concentration of OD<sub>600</sub> = 0.03 for each construct. *N. benthamiana* plants (4-6 week-old) were infiltrated by leaf injection. Duplicate infiltrations were performed on two separate plants per assay in each independent experiment. 48h post-infiltration, small regions of the leaf were excised with a razor blade and mounted in water for imaging.

**Live cell imaging**—Live cell imaging for all figures was conducted using a Nikon Ti-E equipped with an Andor Revolution CSU-W1 spinning disk, a Borealis homogeneous illumination system, an Andor FRAPPA photobleaching unit, an Andor Ixon Ultra 888 EM-CCD and 100x or 60x N.A. 1.49 Apo TIRF oil-immersion objectives. GFP was excited with a 488 nm laser and emission collected with a 525/50 nm band pass filter, YFP was excited with a 515 nm laser and emission collected with a 535/30 nm filter, CFP and mTurquoise were excited with a 445 nm laser and emission collected with a 470/24 nm filter, tdTomato, mCherry and RFP were excited with a 561 nm laser and emission collected with a 610/40 nm filter. Alternatively, some images for quantification were collected with a Nikon Ti-E equipped with an Andor CSU-X1 spinning disk, a BioVision iLAS FRAP photobleaching unit, a Photometrics Evolve EM-CCD and a 100x N.A. 1.49 Apo TIRF oil-immersion objective; with this setup, GFP and YFP were excited with a 491 nm laser and emission collected with a 525/50 nm filter and tdTomato, mCherry and RFP were excited with a 561 nm laser and emission collected with a 595/50 nm filter.

For seedling imaging, 3-day-old etiolated hypocotyls or roots were mounted in water under a pad of 0.8% agarose (Bioline). To limit the time that seedlings spent mounted, no more than three cells per seedling were imaged in any experiment. For short-term inhibitor treatments, seedlings were incubated for the time indicated, gently shaking in a 6-well plate containing ½ MS media with 1% sucrose and 2.5 mM MES pH 5.8, supplemented with 100 nM isoxaben (from a 20 µM stock in ethanol) or 5 µM 2,6-Dichlorobenzonitrile (DCB) (from a 20 µM stock in ethanol), or 100 µM Brefeldin A (BFA) (from a 100 mM stock in DMSO), then mounted in the same medium under an agarose pad as described above.

For FM4-64 uptake assays, seedlings for short time points were directly mounted in water containing 4  $\mu\text{M}$  FM4-64 (from a 4 mM stock in DMSO), while seedlings for long time points were incubated in 4  $\mu\text{M}$  FM4-64 in water for 5 minutes, then transferred to a 6-well plate containing  $\frac{1}{2}$  MS media with 1% sucrose and 2.5 mM MES pH 5.8 for the remainder of the time point before mounting and imaging. FM4-64 signal was excited with a 488 nm laser and emission collected with a 625/90 nm filter.

CESAs were monitored using 10 second time-lapse images for 10 minutes. If required, time-lapse images were aligned using the StackReg plugin (Thévenaz et al., 1998) in Fiji (Schindelin et al., 2012) and background was subtracted from images using a 50 pixel rolling ball radius. Sum projections of time-lapse images were used to select CSC tracks, then kymographs (3 pixel line width) were generated from the time series using the MultiKymograph tool. CSC speeds were calculated from the displacement over time of individual particles identified in the kymographs (Paredez et al., 2006). CSC density at the plasma membrane and SmaCCs in the cell cortex were identified using the ThunderSTORM plugin (Ovesný et al., 2014) with the microscope hardware information, but otherwise using default settings. Golgi bodies in the cell cortex were manually excluded by their large size, SmaCCs were identified as high-intensity particles and the remainder of the particles were considered to be CSCs.

Photobleaching was conducted with an Andor FRAPPA unit on the microscope described above, using the 488 nm laser, a 20 ms dwell time and 80% laser power; otherwise, imaging conditions were as described above for CESA monitoring. New CSC delivery events were identified according to Sampathkumar et al. (2013).

Colocalization was quantified from z-stacks (with 0.2  $\mu\text{m}$  spacing using the 100x N.A. 1.49 objective) using the object-based (centre-particle) method in the JaCOP plugin for Fiji (Bolte and Cordelières, 2006) with the microscope hardware information, but otherwise default settings.

**Transmission electron microscopy**—Etiolated 3-day-old seedlings were cryofixed using a Leica EM-ICE high pressure freezer using B-type carriers and 1-hexadecene as a cryoprotectant, according to McFarlane et al. (2008). Samples were freeze-substituted in a Leica AFS2 automatic freeze substitution unit at  $-85^{\circ}\text{C}$  for 4 days in 2% (w/v) osmium tetroxide (Electron Microscopy Sciences) and 8% 2,2-dimethoxypropane (w/v) in anhydrous acetone, after which the temperature was gradually raised to room temperature over 2 days. Samples were washed 5 times with anhydrous acetone, then infiltrated with Spurr's Resin (Electron Microscopy Sciences) over the course of 4 days. Samples in resin were polymerized at  $65^{\circ}\text{C}$  for 36 hours in BEEM capsules (Electron Microscopy Sciences). Silver ( $\sim 80$  nm thick) sections were cut using a Leica UCT R or a UC7 Ultramicrotome and a DiATOME diamond knife, placed on Gilder fine bar hexagonal 200 mesh grids coated with 0.3% formvar (Electron Microscopy Sciences). Grids were post-stained with 1% aqueous uranyl acetate (Polysciences) and Sato's triple lead (sodium citrate, lead acetate, lead citrate from BDH, lead nitrate from Fisher) and imaged with a Phillips CM120 BioTWIN transmission electron microscope with a Gatan MultiScan 791 CCD camera and a tungsten filament at an accelerating voltage of 120 kV.

**Scanning electron microscopy**—Etiolated 3-day-old seedlings were mounted on a sample holder using Tissue-Tek (Sakura-Finetek), plunge-frozen in a slush of liquid nitrogen (~-210°C), then transferred to a Gatan cryostage. Ice crystals were evaporated at -95°C for 2.5 minutes, then samples were coated with 60:40 gold-palladium alloy for 120 sec (~6 nm) under argon at -120°C, before being transferred into the FEI Quanta cryo scanning electron microscope. Stage temperatures were maintained below -120°C and images were collected at a 5 kV accelerating voltage and a 10 mm working distance using the E-T detector.

**Cell wall analysis**—Cell wall analysis was conducted according to the protocol described in Sánchez-Rodríguez et al. (2012) without any modifications.

**Gene coexpression analysis**—Co-expression analyses were done in two ways. First FamNet (<http://aranet.mpimp-golm.mpg.de/famnet.html>) was used to probe which pfams were associated with cellulose synthesis. Here, “Cellulose\_synth” was used as search term (Figure S1A). We next used PlaNet (<http://aranet.mpimp-golm.mpg.de/index.html>) to investigate what genes from the pfams that were closely co-expressed with the primary wall *CESAs*. Here, we used *CESA1* (At4g32410) as search term. The At5g18520 (*7TMI*) gene was most highly co-expressed with *CESA1* of the members of the Lung\_7-TM\_R pfam (Figure S1B).

**Phylogenetic analysis**—Full length protein sequences were analyzed using MEGA X (Kumar et al., 2018) and included software packages. Sequences were aligned using MUSCLE and unrooted phylogenetic trees were constructed via the Maximum Likelihood method using 391 positions after complete deletion of gaps and missing data. The reliability of the inferred tree was evaluated using 100 bootstrap replicates.

## QUANTIFICATION AND STATISTICAL ANALYSIS

For seedling growth assays, plates were scanned using an Epson 1000XL flat-bed scanner and root or hypocotyl lengths were measured using a segmented line in Fiji (Schindelin et al., 2012).

FM4-64 signal in the plasma membrane was measured in Fiji from a segmented line drawn around the cell (thickness 3 pixels), while intracellular signal was measured from a polygon drawn inside the plasma membrane. Puncta/area of the cell were measured within this same polygon.

Plasma membrane localized *CESAs* were monitored using 10 second time-lapse images for 10 minutes. If required, time-lapse images were aligned using the StackReg plugin (Thévenaz et al., 1998) and background was subtracted from images using a 50 pixel rolling ball radius. Sum projections of time-lapse images were used to select CSC tracks, then kymographs (3 pixel line width) were generated from the time series using the MultiKymograph tool. CSC speeds were calculated from the displacement over time of individual particles identified in the kymographs (Paredes et al., 2006). CSC density at the plasma membrane and SmaCCs in the cell cortex were identified using the ThunderSTORM plugin (Ovesný et al., 2014) with the microscope hardware information, but otherwise using default settings. Golgi bodies in the cell cortex were manually excluded by their large size,

SmaCCs were identified as high-intensity particles and the remainder of the particles were considered to be CSCs. For FRAP experiments, new CSC delivery events were identified according to Sampathkumar et al. (2013).

Colocalization was quantified from z-stacks (with 0.2  $\mu\text{m}$  spacing using the 100x N.A. 1.49 objective) using the object-based (centre-particle) method in the JaCOP plugin for Fiji (Bolte and Cordelières, 2006) with the microscope hardware information, but otherwise default settings.

Box plots and violin plots were prepared using BoxPlotR (Spitzer et al., 2014), bar charts were prepared in Excel. In violin plots, white circles show the medians, wide bar limits indicate the 25<sup>th</sup> and 75<sup>th</sup> percentiles, whiskers extend 1.5 times the interquartile range, polygons represent density estimates of data and extend to extreme values. In box plots, box limits indicate 25<sup>th</sup> and 75<sup>th</sup> percentiles, whiskers extend to 1.5 times the interquartile range, median is indicated by a line, mean by a red “+” and individual data points are shown. In bar charts, bars represent mean, whiskers represent standard error. Unless noted otherwise (in figure legends), graphs summarize data from three independent experiments. For growth assays, n indicates the number of seedlings measured. For cell wall analysis, n indicates distinct pools of seedlings that were homogenized for cell wall extraction. For live cell imaging, n indicates the number of cells quantified for any given measurement; to limit the time that seedlings spent mounted for imaging, no more than three cells per seedling were imaged in any experiment. Details of statistical analysis and number of quantified entities (n) can be found in the figure legends.

## Supplementary Material

Refer to Web version on PubMed Central for supplementary material.

## ACKNOWLEDGMENTS

Live cell imaging was conducted using instruments that are part of the Biological Optical Microscopy Platform (BOMP) at University of Melbourne and electron microscopy was conducted using instruments that are part of the Melbourne Advanced Microscopy Facility. S.P. acknowledges the financial aid of an Australian Research Council (ARC) Discovery grant (DP19001941), Villum Investigator (project ID: 25915), and Novo Nordisk Laureate (NNF19OC0056076) grants. H.E.M. acknowledges an EMBO-LTF (1246-2013), Natrual Sciences and Engineering Council (NSERC) PDF (454454-2014), and an ARC Discovery Early Career Researcher award (DE170100054). J.M.A. acknowledges support from NSF grant IOS1444561, D.M.-A. acknowledges financial support from Deutsche Forschungsgemeinschaft and T.E.G., S.M.A., and D.C. acknowledge support from the U.S. National Science Foundation (MCB-1121612, with additional support from MCB-1715826) and from the National Institute of General Medical Sciences of the NIH under award number R01GM126079. The content is solely the responsibility of the authors and does not necessarily represent the official views of the NIH.

## REFERENCES

- Amsbury S, Hunt L, Elhaddad N, Baillie A, Lundgren M, Verhertbruggen Y, Scheller HV, Knox JP, Fleming AJ, and Gray JE (2016). Stomatal function requires pectin de-methyl-esterification of the guard cell wall. *Curr. Biol* 26, 2899–2906. [PubMed: 27720618]
- Anderson CT, and Kieber JJ (2020). Dynamic Construction, perception, and remodeling of plant cell walls. *Annu. Rev. Plant Biol* 71, 39–69. [PubMed: 32084323]
- Anderson DJ, and Botella JR (2007). Expression analysis and subcellular localization of the *Arabidopsis thaliana* G-protein beta-subunit AGB1. *Plant Cell Rep.* 26, 1469–1480. [PubMed: 17492287]

- Aranda-Sicilia MN, Trusov Y, Maruta N, Chakravorty D, Zhang Y, and Botella JR (2015). Heterotrimeric G proteins interact with defense-related receptor-like kinases in Arabidopsis. *J. Plant Physiol* 188, 44–48. [PubMed: 26414709]
- Arioli T, Peng L, Betzner AS, Burn J, Wittke W, Herth W, Camilleri C, Höfte H, Plazinski J, Birch R, et al. (1998). Molecular analysis of cellulose biosynthesis in Arabidopsis. *Science* 279, 717–720. [PubMed: 9445479]
- Baltoumas FA, Theodoropoulou MC, and Hamodrakas SJ (2013). Interactions of the  $\alpha$ -subunits of heterotrimeric G-proteins with GPCRs, effectors and RGS proteins: a critical review and analysis of interacting surfaces, conformational shifts, structural diversity and electrostatic potentials. *J. Struct. Biol* 182, 209–218. [PubMed: 23523730]
- Bolte S, and Cordelières FP (2006). A guided tour into subcellular colocalization analysis in light microscopy. *J. Microsc* 224, 213–232. [PubMed: 17210054]
- Bommert P, Je BI, Goldshmidt A, and Jackson D (2013). The maize  $G\alpha$  gene COMPACT PLANT2 functions in CLAVATA signalling to control shoot meristem size. *Nature* 502, 555–558. [PubMed: 24025774]
- Brumos J, Zhao C, Gong Y, Soriano D, Patel AP, Perez-Amador MA, Stepanova AN, and Alonso JM (2020). An improved recombineering toolset for plants. *Plant Cell* 32, 100–122. [PubMed: 31666295]
- Chakravorty D, Gookin TE, Milner MJ, Yu Y, and Assmann SM (2015). Extra-large G proteins expand the repertoire of subunits in Arabidopsis heterotrimeric G protein signaling. *Plant Physiol.* 169, 512–529. [PubMed: 26157115]
- Chakravorty D, Trusov Y, Zhang W, Acharya BR, Sheahan MB, McCurdy DW, Assmann SM, and Botella JR (2011). An atypical heterotrimeric G-protein  $\gamma$ -subunit is involved in guard cell  $K^+$ -channel regulation and morphological development in Arabidopsis thaliana. *Plant J.* 67, 840–851. [PubMed: 21575088]
- Chan J, and Coen E (2020). Interaction between autonomous and microtubule guidance systems controls cellulose synthase trajectories. *Curr. Biol* 30, 941–947.e2. [PubMed: 32037093]
- Chen JG, Willard FS, Huang J, Liang J, Chasse SA, Jones AM, and Siderovski DP (2003). A seven-transmembrane RGS protein that modulates plant cell proliferation. *Science* 301, 1728–1731. [PubMed: 14500984]
- Crowell EF, Bischoff V, Desprez T, Rolland A, Stierhof YD, Schumacher K, Gonneau M, Höfte H, and Vernhettes S (2009). Pausing of Golgi bodies on microtubules regulates secretion of cellulose synthase complexes in Arabidopsis. *Plant Cell* 21, 1141–1154. [PubMed: 19376932]
- Curtis MD, and Grossniklaus U (2003). A gateway cloning vector set for high-throughput functional analysis of genes in planta. *Plant Physiol.* 133, 462–469. [PubMed: 14555774]
- Cutler SR, Ehrhardt DW, Griffiths JS, and Somerville CR (2000). Random GFP::cDNA fusions enable visualization of subcellular structures in cells of Arabidopsis at a high frequency. *Proc. Natl. Acad. Sci. USA* 97, 3718–3723. [PubMed: 10737809]
- DeBolt S, Gutierrez R, Ehrhardt DW, and Somerville C (2007). Nonmotile cellulose synthase subunits repeatedly accumulate within localized regions at the plasma membrane in Arabidopsis hypocotyl cells following 2,6-dichlorobenzonitrile treatment. *Plant Physiol.* 145, 334–338. [PubMed: 17911650]
- Delgado-Cerezo M, Sánchez-Rodríguez C, Escudero V, Miedes E, Fernández PV, Jordá L, Hernández-Blanco C, Sánchez-Vallet A, Bednarek P, Schulze-Lefert P, et al. (2012). Arabidopsis heterotrimeric G-protein regulates cell wall defense and resistance to necrotrophic fungi. *Mol. Plant* 5, 98–114. [PubMed: 21980142]
- Denness L, McKenna JF, Segonzac C, Wormit A, Madhou P, Bennett M, Mansfield J, Zipfel C, and Hamann T (2011). Cell wall damage-induced lignin biosynthesis is regulated by a reactive oxygen species- and jasmonic acid-dependent process in Arabidopsis. *Plant Physiol.* 156, 1364–1374. [PubMed: 21546454]
- Desprez T, Juraniec M, Crowell EF, Jouy H, Pochylova Z, Parcy F, Höfte H, Gonneau M, and Vernhettes S (2007). Organization of cellulose synthase complexes involved in primary cell wall synthesis in Arabidopsis thaliana. *Proc. Natl. Acad. Sci. USA* 104, 15572–15577. [PubMed: 17878303]

- Dettmer J, Hong-Hermesdorf A, Stierhof YD, and Schumacher K (2006). Vacuolar H<sup>+</sup>-ATPase activity is required for endocytic and secretory trafficking in Arabidopsis. *Plant Cell* 18, 715–730. [PubMed: 16461582]
- Dunkley TP, Hester S, Shadforth IP, Runions J, Weimar T, Hanton SL, Griffin JL, Bessant C, Brandizzi F, Hawes C, et al. (2006). Mapping the Arabidopsis organelle proteome. *Proc. Natl. Acad. Sci. USA* 103, 6518–6523. [PubMed: 16618929]
- Endler A, Kesten C, Schneider R, Zhang Y, Ivakov A, Froehlich A, Funke N, and Persson S (2015). A mechanism for sustained cellulose synthesis during salt stress. *Cell* 162, 1353–1364. [PubMed: 26343580]
- Escudero V, Jordá L, Sopena-Torres S, Mélida H, Miedes E, Muñoz-Barrios A, Swami S, Alexander D, McKee LS, Sánchez-Vallet A, et al. (2017). Alteration of cell wall xylan acetylation triggers defense responses that counterbalance the immune deficiencies of plants impaired in the  $\beta$ -subunit of the heterotrimeric G-protein. *Plant J.* 92, 386–399. [PubMed: 28792629]
- Fagard M, Desnos T, Desprez T, Goubet F, Refregier G, Mouille G, McCann M, Rayon C, Vernhettes S, and Höfte H (2000). PROCUSTE1 encodes a cellulose synthase required for normal cell elongation specifically in roots and dark-grown hypocotyls of Arabidopsis. *Plant Cell* 12, 2409–2424. [PubMed: 11148287]
- Fan LM, Zhang W, Chen JG, Taylor JP, Jones AM, and Assmann SM (2008). Abscisic acid regulation of guard-cell K<sup>+</sup> and anion channels in G $\beta$ - and RGS-deficient Arabidopsis lines. *Proc. Natl. Acad. Sci. USA* 105, 8476–8481. [PubMed: 18541915]
- Feng W, Kita D, Peaucelle A, Cartwright HN, Doan V, Duan Q, Liu MC, Maman J, Steinhorst L, Schmitz-Thom I, et al. (2018). The FERONIA receptor kinase maintains cell-wall integrity during salt stress through Ca<sup>2+</sup> signaling. *Curr. Biol.* 28, 666–675.e5. [PubMed: 29456142]
- Geldner N, Dénervaud-Tendon V, Hyman DL, Mayer U, Stierhof YD, and Chory J (2009). Rapid, combinatorial analysis of membrane compartments in intact plants with a multicolor marker set. *Plant J.* 59, 169–178. [PubMed: 19309456]
- Gendre D, McFarlane HE, Johnson E, Mouille G, Sjödin A, Oh J, Levesque-Tremblay G, Watanabe Y, Samuels L, and Bhalerao RP (2013). trans-Golgi network localized ECHIDNA/Ypt interacting protein complex is required for the secretion of cell wall polysaccharides in Arabidopsis. *Plant Cell* 25, 2633–2646. [PubMed: 23832588]
- Gonneau M, Desprez T, Martin M, Doblaz VG, Bacete L, Miart F, Sormani R, Hématy K, Renou J, Landrein B, et al. (2018). Receptor kinase THESEUS1 is a rapid alkalization Factor 34 receptor in Arabidopsis. *Curr. Biol.* 28, 2452–2458.e4. [PubMed: 30057301]
- Gookin TE, and Assmann SM (2014). Significant reduction of BiFC non-specific assembly facilitates in planta assessment of heterotrimeric G-protein interactors. *Plant J* 80, 553–567. [PubMed: 25187041]
- Gookin TE, Kim J, and Assmann SM (2008). Whole proteome identification of plant candidate G-protein coupled receptors in Arabidopsis, rice, and poplar: computational prediction and in-vivo protein coupling. *Genome Biol.* 9, R120. [PubMed: 18671868]
- Grebe M, Xu J, Möbius W, Ueda T, Nakano A, Geuze HJ, Rook MB, and Scheres B (2003). Arabidopsis sterol endocytosis involves actin-mediated trafficking via ARA6-positive early endosomes. *Curr. Biol* 13, 1378–1387. [PubMed: 12932321]
- Grefen C, Donald N, Hashimoto K, Kudla J, Schumacher K, and Blatt MR (2010). A ubiquitin-10 promoter-based vector set for fluorescent protein tagging facilitates temporal stability and native protein distribution in transient and stable expression studies. *Plant J.* 64, 355–365. [PubMed: 20735773]
- Groen AJ, Sancho-Andrés G, Breckels LM, Gatto L, Aniento F, and Lilley KS (2014). Identification of trans-Golgi network proteins in Arabidopsis thaliana root tissue. *J. Proteome Res* 13, 763–776. [PubMed: 24344820]
- Gutierrez R, Lindeboom JJ, Paredez AR, Emons AM, and Ehrhardt DW (2009). Arabidopsis cortical microtubules position cellulose synthase delivery to the plasma membrane and interact with cellulose synthase trafficking compartments. *Nat. Cell Biol.* 11, 797–806. [PubMed: 19525940]
- Haruta M, Sabat G, Stecker K, Minkoff BB, and Sussman MR (2014). A peptide hormone and its receptor protein kinase regulate plant cell expansion. *Science* 343, 408–411. [PubMed: 24458638]

- Heim DR, Skomp JR, Tschabold EE, and Larrinua IM (1990). Isoxaben inhibits the synthesis of acid insoluble cell wall materials in *Arabidopsis thaliana*. *Plant Physiol.* 93, 695–700. [PubMed: 16667525]
- Hématy K, Sado PE, Van Tuinen A, Rochange S, Desnos T, Balzergue S, Pelletier S, Renou JP, and Höfte H (2007). A receptor-like kinase mediates the response of *Arabidopsis* cells to the inhibition of cellulose synthesis. *Curr. Biol* 17, 922–931. [PubMed: 17540573]
- Hirata T, Fujita M, Nakamura S, Gotoh K, Motooka D, Murakami Y, Maeda Y, and Kinoshita T (2015). Post-Golgi anterograde transport requires GARP-dependent endosome-to-TGN retrograde transport. *Mol. Biol. Cell* 26, 3071–3084. [PubMed: 26157166]
- Hoffmann N, King S, Samuels AL, and McFarlane HE (2021). Subcellular coordination of plant cell wall synthesis. *Dev. Cell* 56, 933–948. [PubMed: 33761322]
- Jaffé FW, Freschet GE, Valdes BM, Runions J, Terry MJ, and Williams LE (2012). G protein-coupled receptor-type G proteins are required for light-dependent seedling growth and fertility in *Arabidopsis*. *Plant Cell* 24, 3649–3668. [PubMed: 23001037]
- Jefferson RA, Kavanagh TA, and Bevan MW (1987). GUS fusions: beta-glucuronidase as a sensitive and versatile gene fusion marker in higher plants. *EMBO J.* 6, 3901–3907. [PubMed: 3327686]
- Jones AM, Ecker JR, and Chen JG (2003). A reevaluation of the role of the heterotrimeric G protein in coupling light responses in *Arabidopsis*. *Plant Physiol.* 131, 1623–1627. [PubMed: 12692321]
- Kloppfleisch K, Phan N, Augustin K, Bayne RS, Booker KS, Botella JR, Carpita NC, Carr T, Chen JG, Cooke TR, et al. (2011). *Arabidopsis* G-protein interactome reveals connections to cell wall carbohydrates and morphogenesis. *Mol. Syst. Biol* 7, 532. [PubMed: 21952135]
- Kohorn BD, and Kohorn SL (2012). The cell wall-associated kinases, WAKs, as pectin receptors. *Front. Plant Sci* 3, 88. [PubMed: 22639672]
- Kumar S, Stecher G, Li M, Knyaz C, and Tamura K (2018). MEGA X: Molecular evolutionary genetics analysis across computing platforms. *Mol. Biol. Evol* 35, 1547–1549. [PubMed: 29722887]
- Liang X, Ding P, Lian K, Wang J, Ma M, Li L, Li L, Li M, Zhang X, Chen S, et al. (2016). *Arabidopsis* heterotrimeric G proteins regulate immunity by directly coupling to the FLS2 receptor. *eLife* 5, e13568. [PubMed: 27043937]
- Maruta N, Trusov Y, Chakravorty D, Urano D, Assmann SM, and Botella JR (2019). Nucleotide exchange-dependent and nucleotide exchange-independent functions of plant heterotrimeric GTP-binding proteins. *Sci. Signal* 12, eaav9526. [PubMed: 31690635]
- McFarlane HE, Döring A, and Persson S (2014). The cell biology of cellulose synthesis. *Annu. Rev. Plant Biol* 65, 69–94. [PubMed: 24579997]
- McFarlane HE, Young RE, Wasteneys GO, and Samuels AL (2008). Cortical microtubules mark the mucilage secretion domain of the plasma membrane in *Arabidopsis* seed coat cells. *Planta* 227, 1363–1375. [PubMed: 18309515]
- Munk C, Mutt E, Isberg V, Nikolajsen LF, Bibbe JM, Flock T, Hanson MA, Stevens RC, Deupi X, and Gloriam DE (2019). An online resource for GPCR structure determination and analysis. *Nat. Methods* 16, 151–162. [PubMed: 30664776]
- Obayashi T, Aoki Y, Tadaka S, Kagaya Y, and Kinoshita K (2018). ATTED-II in 2018: a plant coexpression database based on investigation of the statistical property of the mutual rank index. *Plant Cell Physiol.* 59, e3. [PubMed: 29216398]
- Ovesný M, Křížek P, Borkovec J, Svindrych Z, and Hagen GM (2014). ThunderSTORM: a comprehensive ImageJ plug-in for PALM and STORM data analysis and super-resolution imaging. *Bioinformatics* 30, 2389–2390. [PubMed: 24771516]
- Pandey S (2019). Heterotrimeric G-protein signaling in plants: conserved and novel mechanisms. *Annu. Rev. Plant Biol* 70, 213–238. [PubMed: 31035831]
- Paredez AR, Somerville CR, and Ehrhardt DW (2006). Visualization of cellulose synthase demonstrates functional association with microtubules. *Science* 312, 1491–1495. [PubMed: 16627697]
- Parsons HT, Christiansen K, Knierim B, Carroll A, Ito J, Batth TS, Smith-Moritz AM, Morrison S, McInerney P, Hadi MZ, et al. (2012). Isolation and proteomic characterization of the *Arabidopsis*

- Golgi defines functional and novel components involved in plant cell wall biosynthesis. *Plant Physiol.* 159, 12–26. [PubMed: 22430844]
- Persson S, Paredez A, Carroll A, Palsdottir H, Doblin M, Poindexter P, Khitrov N, Auer M, and Somerville CR (2007). Genetic evidence for three unique components in primary cell-wall cellulose synthase complexes in *Arabidopsis*. *Proc. Natl. Acad. Sci. USA* 104, 15566–15571. [PubMed: 17878302]
- Persson S, Wei H, Milne J, Page GP, and Somerville CR (2005). Identification of genes required for cellulose synthesis by regression analysis of public microarray data sets. *Proc. Natl. Acad. Sci. USA* 102, 8633–8638. [PubMed: 15932943]
- Polko JK, Barnes WJ, Voiniciuc C, Doctor S, Steinwand B, Hill JL Jr., Tien M, Pauly M, Anderson CT, and Kieber JJ (2018). SHOU4 proteins regulate trafficking of cellulose synthase complexes to the plasma membrane. *Curr. Biol* 28, 3174–3182.e6. [PubMed: 30245104]
- Richter S, Geldner N, Schrader J, Wolters H, Stierhof YD, Rios G, Koncz C, Robinson DG, and Jürgens G (2007). Functional diversification of closely related ARF-GEFs in protein secretion and recycling. *Nature* 448, 488–492. [PubMed: 17653190]
- Roy Choudhury S, Marlin MA, and Pandey S (2019). The role of G $\beta$  protein in controlling cell expansion via potential interaction with lipid metabolic pathways. *Plant Physiol.* 179, 1159–1175. [PubMed: 30622152]
- Rui Y, and Dinneny JR (2020). A wall with integrity: surveillance and maintenance of the plant cell wall under stress. *New Phytol.* 225, 1428–1439. [PubMed: 31486535]
- Rui Y, Xiao C, Yi H, Kandemir B, Wang JZ, Puri VM, and Anderson CT (2017). Polygalacturonase INVOLVED IN EXPANSION3 Functions in Seedling Development, Rosette Growth, and stomatal Dynamics in *Arabidopsis thaliana*. *Plant Cell* 29, 2413–2432. [PubMed: 28974550]
- Ruprecht C, Mendrinna A, Tohge T, Sampathkumar A, Klie S, Fernie AR, Nikoloski Z, Persson S, and Mutwil M (2016). FamNet: a framework to identify multiplied modules driving pathway expansion in plants. *Plant Physiol.* 170, 1878–1894. [PubMed: 26754669]
- Saint-Jore-Dupas C, Nebenführ A, Boulaflous A, Follet-Gueye ML, Plasson C, Hawes C, Driouich A, Faye L, and Gomord V (2006). Plant N-glycan processing enzymes employ different targeting mechanisms for their spatial arrangement along the secretory pathway. *Plant Cell* 18, 3182–3200. [PubMed: 17138701]
- Samalova M, Fricker M, and Moore I (2006). Ratiometric fluorescence-imaging assays of plant membrane traffic using polyproteins. *Traffic* 7, 1701–1723. [PubMed: 17118121]
- Sampathkumar A, Gutierrez R, McFarlane HE, Bringmann M, Lindeboom J, Emons AM, Samuels L, Ketelaar T, Ehrhardt DW, and Persson S (2013). Patterning and lifetime of plasma membrane-localized cellulose synthase is dependent on actin organization in *Arabidopsis* interphase cells. *Plant Physiol.* 162, 675–688. [PubMed: 23606596]
- Sánchez-Rodríguez C, Bauer S, Hématy K, Saxe F, Ibáñez AB, Vodermaier V, Konlechner C, Sampathkumar A, Rüggeberg M, Aichinger E, et al. (2012). Chitinase-like1/pom-pom1 and its homolog CTL2 are glucan-interacting proteins important for cellulose biosynthesis in *Arabidopsis*. *Plant Cell* 24, 589–607. [PubMed: 22327741]
- Sánchez-Rodríguez C, Estévez JM, Llorente F, Hernández-Blanco C, Jordá L, Pagán I, Berrocal M, Marco Y, Somerville S, and Molina A (2009). The ERECTA receptor-like kinase regulates cell wall-mediated resistance to pathogens in *Arabidopsis thaliana*. *Mol. Plant Microbe Interact.* 22, 953–963. [PubMed: 19589071]
- Sánchez-Rodríguez C, Shi Y, Kesten C, Zhang D, Sancho-Andrés G, Ivakov A, Lampugnani ER, Sklodowski K, Fujimoto M, Nakano A, et al. (2018). The cellulose synthases are cargo of the TPLATE adaptor complex. *Mol. Plant* 11, 346–349. [PubMed: 29221860]
- Schindelin J, Arganda-Carreras I, Frise E, Kaynig V, Longair M, Pietzsch T, Preibisch S, Rueden C, Saalfeld S, Schmid B, et al. (2012). Fiji: an open-source platform for biological-image analysis. *Nat. Methods* 9, 676–682. [PubMed: 22743772]
- Shim I, Law R, Kileeg Z, Stronghill P, Northey JGB, Strap JL, and Bonetta DT (2018). Alleles causing resistance to isoxaben and Flupoxam highlight the significance of transmembrane domains for CESA protein function. *Front. Plant Sci* 9, 1152. [PubMed: 30197649]

- Spitzer M, Wildenhain J, Rappsilber J, and Tyers M (2014). BoxPlotR: a web tool for generation of box plots. *Nat. Methods* 11, 121–122. [PubMed: 24481215]
- Stahelin LA, and Kang BH (2008). Nanoscale architecture of endoplasmic reticulum export sites and of Golgi membranes as determined by electron tomography. *Plant Physiol.* 147, 1454–1468. [PubMed: 18678738]
- Tafesse FG, Guimaraes CP, Maruyama T, Carette JE, Lory S, Brummelkamp TR, and Ploegh HL (2014). GPR107, a G-protein-coupled receptor essential for intoxication by *Pseudomonas aeruginosa* exotoxin A, localizes to the Golgi and is cleaved by furin. *J. Biol. Chem* 289, 24005–24018. [PubMed: 25031321]
- Teh OK, and Moore I (2007). An ARF-GEF acting at the Golgi and in selective endocytosis in polarized plant cells. *Nature* 448, 493–496. [PubMed: 17653191]
- Thévenaz P, Ruttimann UE, and Unser M (1998). A pyramid approach to subpixel registration based on intensity. *IEEE Trans. Image Process.* 7, 27–41. [PubMed: 18267377]
- Thung L, Trusov Y, Chakravorty D, and Botella JR (2012).  $G\gamma 1 + G\gamma 2 + G\gamma 3 = G\beta$ : the search for heterotrimeric G-protein  $\gamma$  subunits in *Arabidopsis* is over. *J. Plant Physiol* 169, 542–545. [PubMed: 22209167]
- Toyooka K, Goto Y, Asatsuma S, Koizumi M, Mitsui T, and Matsuoka K (2009). A mobile secretory vesicle cluster involved in mass transport from the Golgi to the plant cell exterior. *Plant Cell* 21, 1212–1229. [PubMed: 19376937]
- Trusov Y, Rookes JE, Tilbrook K, Chakravorty D, Mason MG, Anderson D, Chen JG, Jones AM, and Botella JR (2007). Heterotrimeric G protein gamma subunits provide functional selectivity in Gbetagamma dimer signaling in *Arabidopsis*. *Plant Cell* 19, 1235–1250. [PubMed: 17468261]
- Tunc-Ozdemir M, Urano D, Jaiswal DK, Clouse SD, and Jones AM (2016). Direct modulation of heterotrimeric G protein-coupled signaling by a receptor kinase complex. *J. Biol. Chem* 291, 13918–13925. [PubMed: 27235398]
- Ullah H, Chen JG, Temple B, Boyes DC, Alonso JM, Davis KR, Ecker JR, and Jones AM (2003). The beta-subunit of the *Arabidopsis* G protein negatively regulates auxin-induced cell division and affects multiple developmental processes. *Plant Cell* 15, 393–409. [PubMed: 12566580]
- Ullah H, Chen JG, Young JC, Im KH, Sussman MR, and Jones AM (2001). Modulation of cell proliferation by heterotrimeric G protein in *Arabidopsis*. *Science* 292, 2066–2069. [PubMed: 11408654]
- Vaahtera L, Schulz J, and Hamann T (2019). Cell wall integrity maintenance during plant development and interaction with the environment. *Nat. Plants* 5, 924–932. [PubMed: 31506641]
- Waese J, Fan J, Pasha A, Yu H, Fucile G, Shi R, Cumming M, Kelley LA, Sternberg MJ, Krishnakumar V, et al. (2017). ePlant: visualizing and exploring multiple levels of data for hypothesis generation in plant biology. *Plant Cell* 29, 1806–1821. [PubMed: 28808136]
- Worden N, Wilkop TE, Esteve VE, Jeannotte R, Lathe R, Vernhettes S, Weimer B, Hicks G, Alonso J, Labavitch J, et al. (2015). CESA TRAFFICKING INHIBITOR inhibits cellulose deposition and interferes with the trafficking of cellulose synthase complexes and their associated proteins KORRIGAN1 and POM2/cellulose synthase INTERACTIVE PROTEIN1. *Plant Physiol.* 167, 381–393. [PubMed: 25535279]
- Yu Y, Chakravorty D, and Assmann SM (2018). The G protein  $\beta$ -subunit, AGB1, interacts with FERONIA in RALF1-regulated stomatal movement. *Plant Physiol.* 176, 2426–2440. [PubMed: 29301953]
- Zeng Q, Wang X, and Running MP (2007). Dual lipid modification of *Arabidopsis*  $G\gamma$ -subunits is required for efficient plasma membrane targeting. *Plant Physiol.* 143, 1119–1131. [PubMed: 17220359]
- Zhang W, Cai C, and Staiger CJ (2019). Myosins XI are involved in exocytosis of cellulose synthase complexes. *Plant Physiol.* 179, 1537–1555. [PubMed: 30705068]
- Zhang Y, Nikolovski N, Sorieul M, Velloso T, McFarlane HE, Dupree R, Kesten C, Schneider R, Driemeier C, Lathe R, et al. (2016). Golgi-localized STELLO proteins regulate the assembly and trafficking of cellulose synthase complexes in *Arabidopsis*. *Nat. Commun* 7, 11656. [PubMed: 27277162]

- Zhou GL, Na SY, Niedra R, and Seed B (2014). Deficits in receptor-mediated endocytosis and recycling in cells from mice with *Gpr107* locus disruption. *J. Cell Sci* 127, 3916–3927. [PubMed: 24849652]
- Zhu C, Ganguly A, Baskin TI, McClosky DD, Anderson CT, Foster C, Meunier KA, Okamoto R, Berg H, and Dixit R (2015). The fragile *Fiber1* kinesin contributes to cortical microtubule-mediated trafficking of cell wall components. *Plant Physiol.* 167, 780–792. [PubMed: 25646318]
- Zhu X, Li S, Pan S, Xin X, and Gu Y (2018). *CSII*, *PATROL1*, and exocyst complex cooperate in delivery of cellulose synthase complexes to the plasma membrane. *Proc. Natl. Acad. Sci. USA* 115, E3578–E3587. [PubMed: 29581258]

**Highlights**

- Members of a 7TM family are required for plant resilience under cell wall stress
- These 7TMs are similar to mammalian G protein-coupled receptors
- 7TMs and G protein complex components interact in the secretory pathway
- 7TMs promote cellulose synthase secretion to fortify the plant cell wall

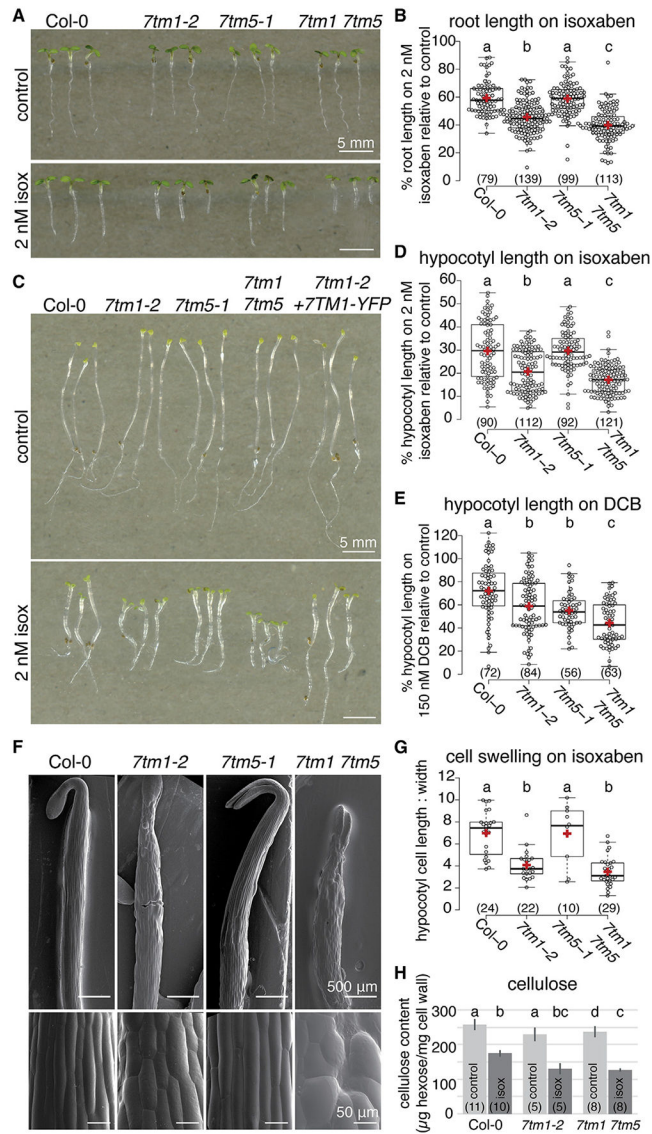


**Figure 1. Mutations in 7TM family members cause increased sensitivity to cell wall stress**  
 (A) Representative images of 7-day-old light-grown seedlings grown on control media and media supplemented with 2 nM isoxaben (isox).  
 (B) Quantification of root lengths of seedlings represented in (A).  
 (C) Representative images of etiolated 7-day-old seedlings grown on control media and media supplemented with 2 nM isoxaben.  
 (D) Quantification of hypocotyl lengths of seedlings represented in (C).  
 (E) Quantification of 7-day-old etiolated hypocotyl lengths of seedlings grown on control media and media supplemented with 150 nM DCB.  
 (F) Cryo-scanning electron microscopy (SEM) of 3-day-old etiolated hypocotyls of seedlings grown on media supplemented with 2 nM isoxaben.  
 (G) Quantification of cell length: width ratio from SEM images as a measure of cell swelling.  
 (H) Quantification of cellulose content in control and isoxaben-treated seedlings.

(H) Quantification of cellulose content in different genotypes. All graphs summarize three independent experiments (two for SEM), n is indicated in parentheses; samples not sharing a common letter are significantly different (one-way ANOVA and Tukey HSD test,  $p < 0.05$ ); in bar charts bars represent mean  $\pm$  SE and in box plots box limits indicate 25<sup>th</sup> and 75<sup>th</sup> percentiles, whiskers extend to 1.5 times the interquartile range, median is indicated by a line, mean by a red “+” and individual data points are shown. Scale bars represent 5 mm in (A and C) and 500 or 50 mm as indicated in (F).

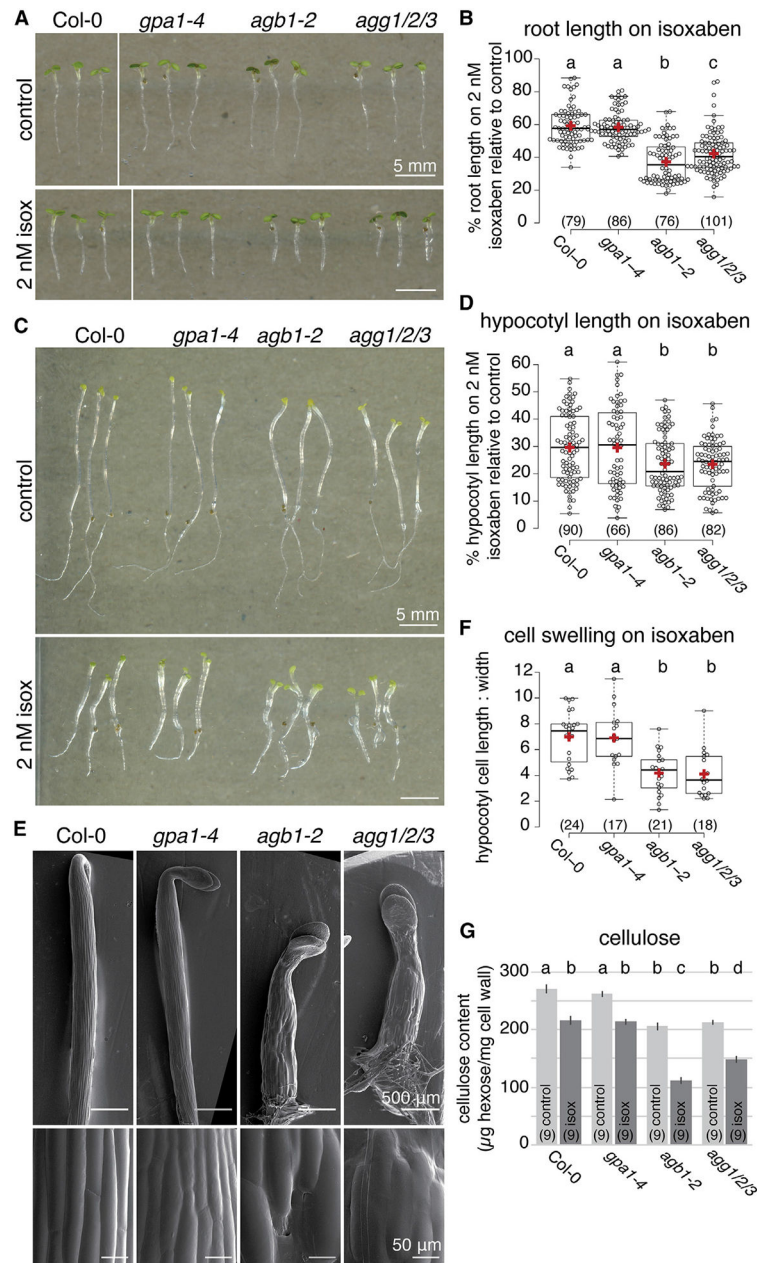


**Figure 2. Mutations in components of the G protein signaling complex cause increased sensitivity to cell wall stress**

(A) Representative images of 7-day-old light-grown seedlings grown on control media and media supplemented with 2 nM isoxaben.

(B) Quantification of root lengths of seedlings represented in A.

(C) Representative images of etiolated 7-day-old seedlings grown on control media and media supplemented with 2 nM isoxaben.

(D) Quantification of hypocotyl lengths of seedlings represented in (B).

(E) Cryo-scanning electron microscopy (SEM) of 3-day-old etiolated hypocotyls of seedlings grown on media supplemented with 2 nM isoxaben.

(F) Quantification of cell length: width ratio from SEM images as a measure of cell swelling.

(G) Quantification of cellulose content in different genotypes. All graphs summarize three independent experiments (two for SEM), Col-0 data in (B, D, and F) are the same as in Figure 1 since all samples were grown together, n is indicated in parentheses; samples not sharing a common letter are significantly different (one-way ANOVA and Tukey HSD test,  $p < 0.05$ ); in bar charts bars represent mean  $\pm$  SE and in box plots box limits indicate 25<sup>th</sup> and 75<sup>th</sup> percentiles, whiskers extend to 1.5 times the interquartile range, median is indicated by a line, mean by a red “+” and individual data points are shown. Scale bars represent 5 mm in (A and C) and 500 or 50  $\mu\text{m}$  as indicated in (E).

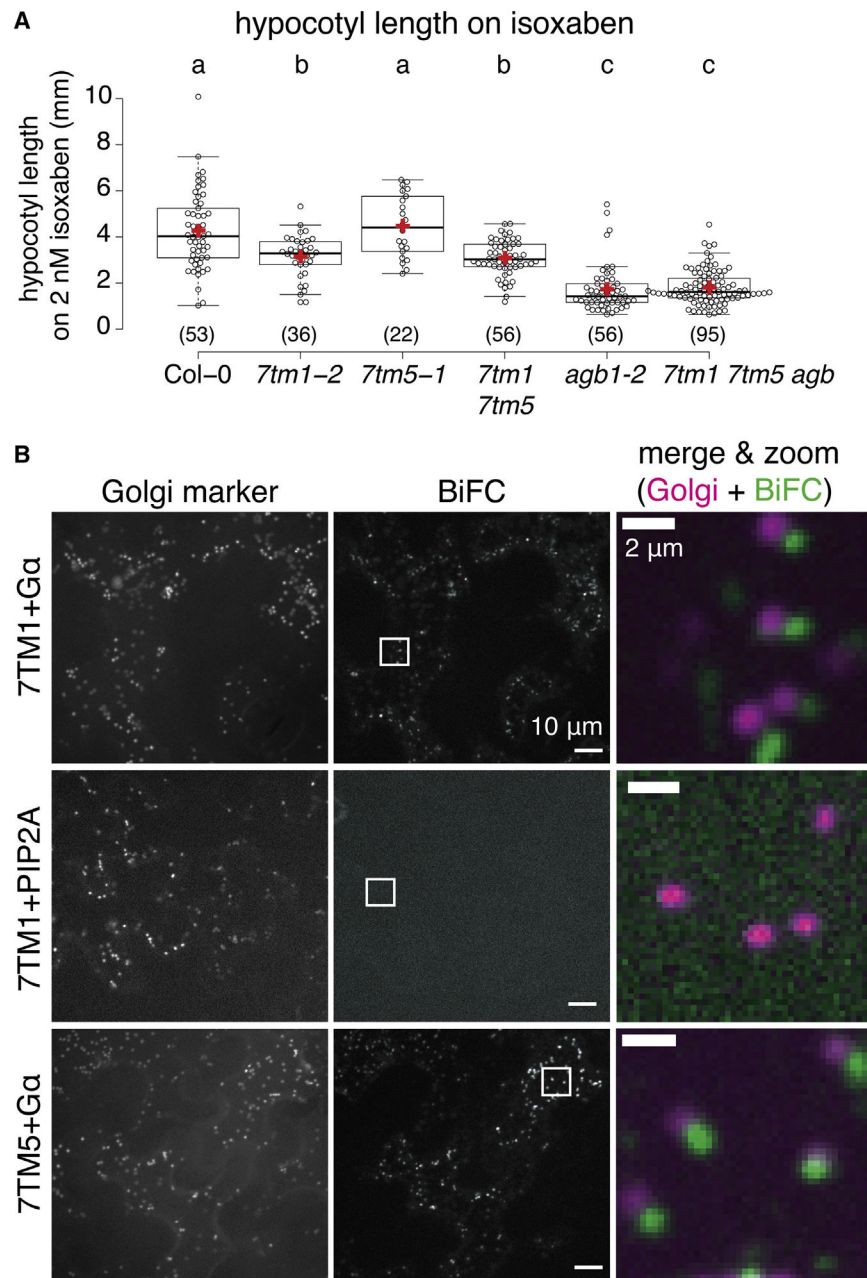


**Figure 3. 7TMs interact with components of the G protein complex**

(A) Quantification of etiolated hypocotyl lengths of combinatorial mutants between the *7tm* mutants and G $\beta$  mutant *agb1-2*.

(B) Bimolecular fluorescence complementation (BiFC) assay in transiently infiltrated *Nicotiana benthamiana* leaf epidermal cells with the BiFC signal shown in green and Golgi marker (XYLT) in magenta in the Merge & Zoom column; white boxes indicate the zoom region. Experiment was repeated three times with similar results. In box plot, box limits indicate 25<sup>th</sup> and 75<sup>th</sup> percentiles, whiskers extend to 1.5 times the interquartile range, median is indicated by a line, mean by a red “+”, individual data points are shown, n is indicated in parentheses and samples not sharing a common letter are significantly different

(one-way ANOVA and Tukey HSD test,  $p < 0.05$ ). Scale bars represent 10 or 2  $\mu\text{m}$  as indicated in (B).

Author Manuscript

Author Manuscript

Author Manuscript

Author Manuscript

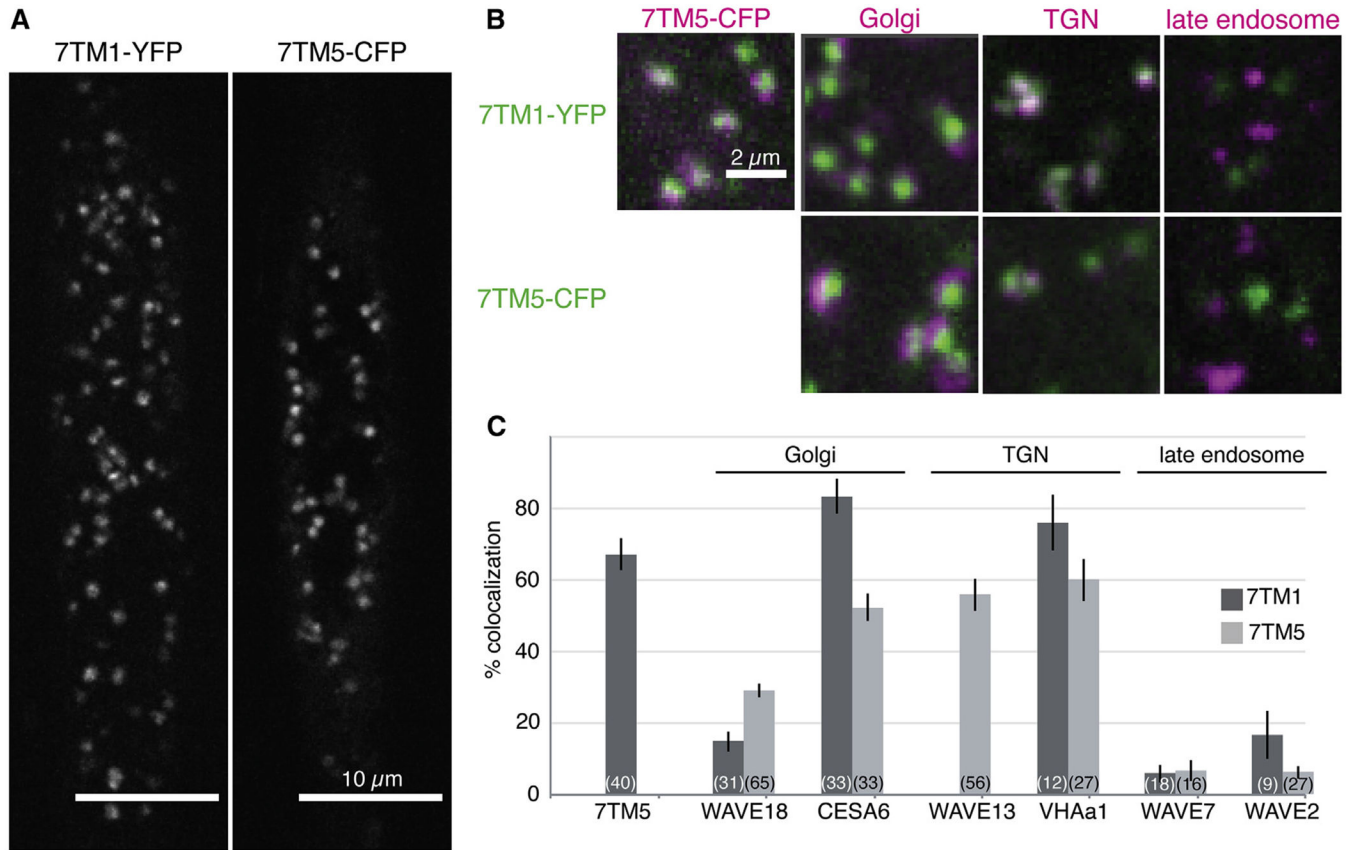


**Figure 4. The 7TMs are localized to the Golgi apparatus and *trans*-Golgi network**  
 (A) Functional 7TM1-YFP (native promoter-driven genomic 7TM1-3xYFP) and 7TM5-CFP (35S-driven) fusion proteins localize to intracellular compartments in 3-day-old etiolated hypocotyl cells.  
 (B) Representative images from colocalization experiments between 7TM1-3xYFP (green) and 7TM5-CFP (magenta) or between 7TM1-3xYFP or 7TM5-CFP (green) and different endomembrane markers (magenta) as indicated in 3-day-old seedling root cells. C. Quantification of percent colocalization between 7TM1-3xYFP, 7TM1-mCherry, or 7TM5-CFP and endomembrane system markers. Graph summarizes three independent experiments, n (cells, no more than three cells imaged per seedling) is indicated in parentheses, bars represent mean  $\pm$  SE Scale bars represent 10  $\mu$ m in (A) and 2  $\mu$ m in (B).

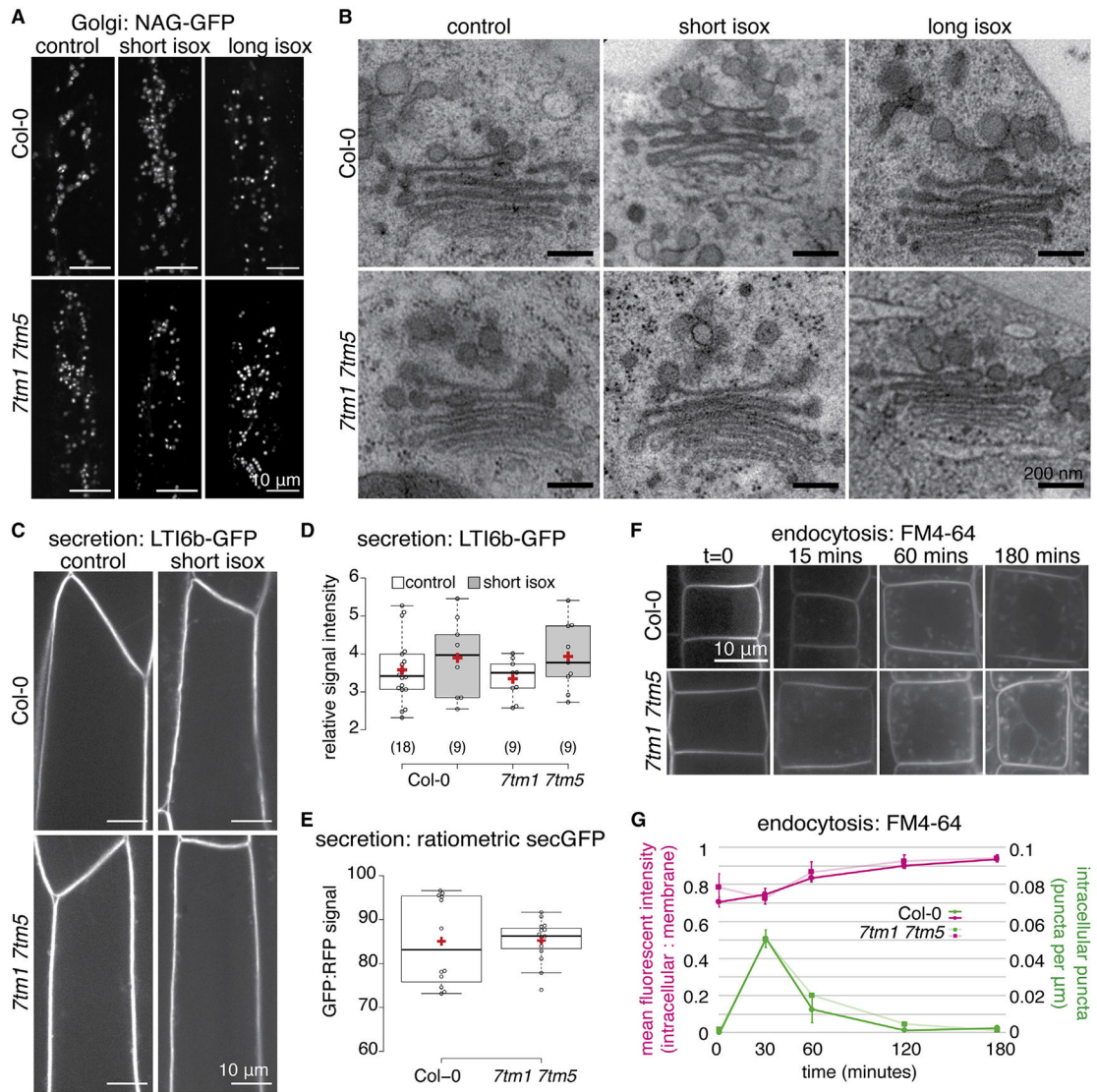


**Figure 5. Overall Golgi structure and function are unaffected in *7tm* mutants**

(A) Representative images of the Golgi marker, NAG-GFP in 3-day-old wild type and *7tm1 7tm5* mutant etiolated hypocotyl cells after short-term (100 nM for 1 h) or long-term (2 nM for 3 days) isoxaben treatment, compared with control.

(B) Representative images of the Golgi apparatus in high-pressure frozen, freeze-substituted 3-day-old wild type and *7tm1 7tm5* mutant etiolated hypocotyl cells after short-term or long-term isoxaben treatment, relative to control.

(C) Representative images of the plasma membrane marker, GFP-LTI6b in 3-day-old wild type and *7tm1 7tm5* mutant etiolated hypocotyl cells after short-term isoxaben treatment.

(D) Quantification of signal intensity from GFP-LTI6b signal represented in (C).

(E) Quantification of ratiometric sec-GFP (35S:stN-RM-2A-sec-GFP) in *7tm1 7tm5* mutants, compared with wild type, in 3-day-old etiolated hypocotyls.

(F) Representative time course images of membrane dye (FM4-64) uptake into in root cells of 3-day-old seedlings of *7tm1 7tm5* mutants, compared with wild type. FM4-64 initially

labels the plasma membrane, then travels to the early endosome/TGN, late endosome and the tonoplast (vacuole membrane) over 3 h.

(G) Quantification of FM4-64 uptake represented in (F). All graphs summarize three independent experiments, n (cells, no more than three cells imaged per seedling) is indicated in parentheses and there were no statistically significant differences between samples (one-way ANOVA and Tukey HSD test,  $p < 0.05$ ). In box plots, box limits indicate 25<sup>th</sup> and 75<sup>th</sup> percentiles, whiskers extend to 1.5 times the interquartile range, median is indicated by a line, mean by a red “+” and individual data points are shown; in line plot, symbols represent mean  $\pm$  SE. Scale bars represent 10  $\mu\text{m}$  in (A, C, F, H) and 200 nm in (B).

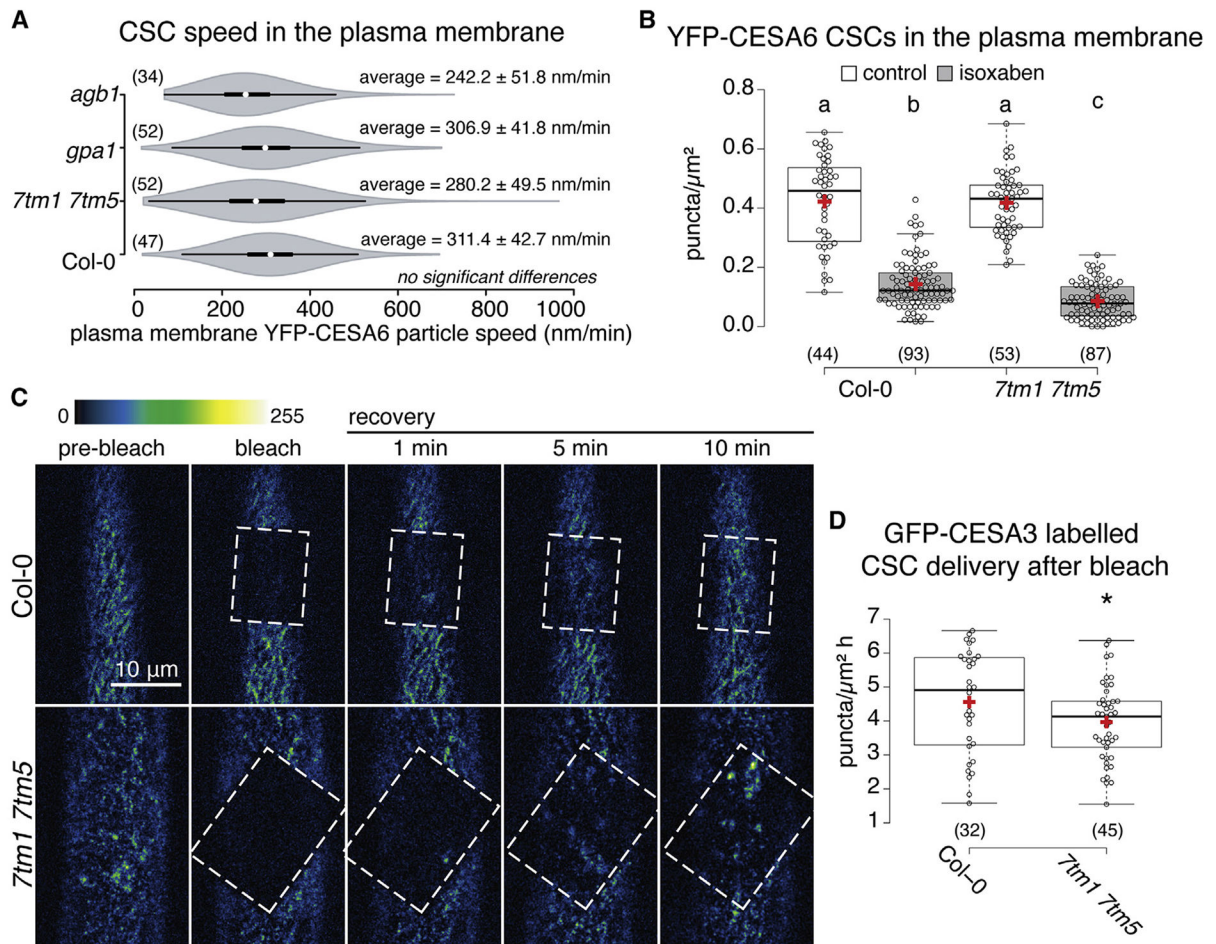


**Figure 6. *7tm* mutants are defective in secretion of CSCs to the plasma membrane**

(A) Quantification of CSC speeds in the plasma membrane of 3-day-old wild type and mutant etiolated hypocotyl cells.

(B) Quantification of YFP-CESA6 labeled CSC particle density in the plasma membrane of 3-day-old etiolated hypocotyl cells in wild type versus *7tm1 7tm5* mutants after control or long-term isoxaben treatment (2 nM for 3 days).

(C) Representative time course images of photobleaching of GFP-CESA3 in wild type and *7tm1 7tm5* mutant 3-day-old etiolated hypocotyl cells. Bleached area is indicated by dashed box, images are false-colored according to the scale indicated.

(D) Quantification of the rate of CSC recovery in the plasma membrane after photobleaching in wild type versus *7tm1 7tm5* mutant 3-day-old etiolated hypocotyl cells. All graphs summarize three independent experiments, n (cells, no more than three cells imaged per seedling) is indicated in parentheses, samples not sharing a common letter in B are significantly different (one-way ANOVA and Tukey HSD test,  $p < 0.05$ ) and in (D) samples marked by an  $\times$  are significantly different from control (one-way t test,  $p < 0.05$ ). In violin plot, white circles show the medians, wide bar limits indicate the 25<sup>th</sup> and 75<sup>th</sup> percentiles, whiskers extend 1.5 times the interquartile range, polygons represent density estimates of data and extend to extreme values. In box plot, box limits indicate 25<sup>th</sup> and 75<sup>th</sup> percentiles,

whiskers extend to 1.5 times the interquartile range, median is indicated by a line, mean by a red “+” and individual data points are shown. Scale bars represent 10  $\mu\text{m}$  in (C).

Author Manuscript

Author Manuscript

Author Manuscript

Author Manuscript

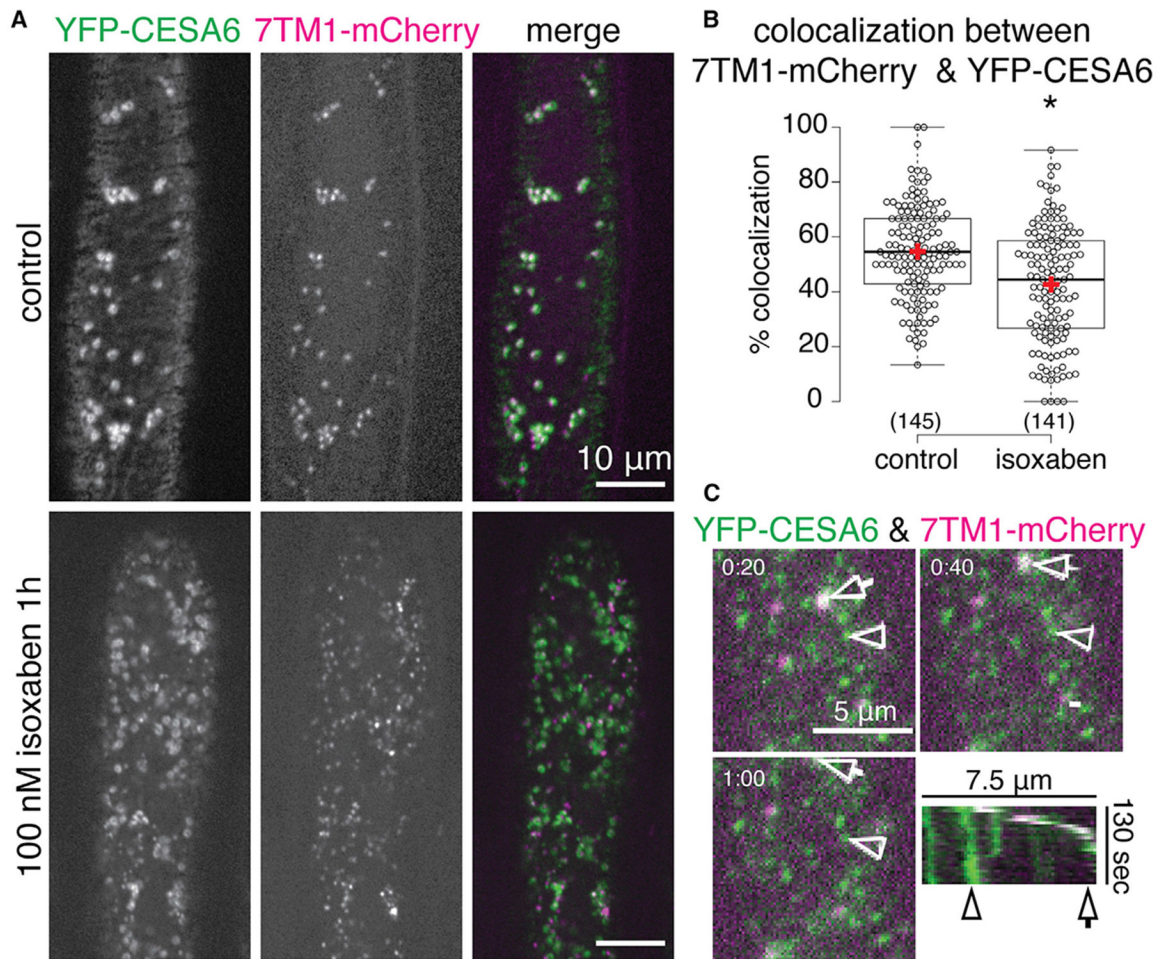


**Figure 7. 7TM1 localization is biased from Golgi/TGN to SmaCCs upon cell wall stress treatment**

(A) Representative images of YFP-CESA6 and 7TM1-mCherry colocalization in 3-day-old etiolated hypocotyl cells after control or short-term (100 nM for 1 h) isoxaben treatment. (B) Quantification of percent colocalization between YFP-CESA6 and 7TM1-mCherry in 3-day-old etiolated hypocotyl cells after control or short-term isoxaben treatment. (C). Representative time-lapse images of YFP-CESA6 and 7TM1-mCherry colocalization in 3-day-old etiolated hypocotyl cells after control or short-term isoxaben treatment and kymograph indicating dynamics of YFP-CESA6 and 7TM1-mCherry labeled particles; timestamp is in minutes:seconds. Graph summarizes three independent experiments, n (cells, no more than three cells imaged per seedling) is indicated in parentheses, samples marked by an  $\times$  are significantly different from control (one-way t test,  $p < 0.05$ ), box limits indicate 25<sup>th</sup> and 75<sup>th</sup> percentiles, whiskers extend to 1.5 times the interquartile range, median is indicated by a line, mean by a red “+” and individual data points are shown. Scale bars represent 10  $\mu\text{m}$  in (A) and 5  $\mu\text{m}$  or 7.5  $\mu\text{m}$  as indicated in (C).

## KEY RESOURCES TABLE

REAGENT or RESOURCE	SOURCE	IDENTIFIER
Bacterial and Virus Strains		
<i>E. coli</i> strain DH alpha	Widely distributed	N/A
<i>E. coli</i> recombineering strain SW105	Brumos et al., 2020	N/A
<i>Agrobacterium tumefaciens</i> strain GV3101	Widely distributed	N/A
Chemicals, Peptides, and Recombinant Proteins		
Murashige and Skoog Medium	Duchefa	Cat# M0222
MES	Sigma	Cat# M8250
isoxaben	Sigma	Cat# 36138
2,6-Dichlorobenzonitrile (DCB)	Sigma	Cat# D57558
Brefeldin A (BFA)	Sigma	Cat# B6542
silwet L-77	PhytoTech Labs	Cat# S7777
acetosyringone	PhytoTech Labs	Cat# A104
1-hexadecene	Sigma	H2131
osmium tetroxide	Electron Microscopy Sciences	Cat# 19100
2,2-dimethoxypropane	Sigma	Cat# D136808
uranyl acetate	Polysciences	Cat# 21447-25
sodium citrate	BDH	Cat# 30152
lead acetate	BDH	Cat# 4578
lead citrate	BDH	Cat# 29726
lead nitrate	Fisher	Cat# S25381
formvar	Electron Microscopy Sciences	Cat# 15800
Tissue-Tek	Electron Microscopy Sciences	Cat# 4583
Other solvents, buffers, and chemicals	Sigma	N/A
Critical Commercial Assays		
RNeasy Plant Mini kit	Qiagen	Cat# 74904
SSVI first strand synthesis kit	Invitrogen	Cat# 18091050
DnaseI (Amp Grade)	Invitrogen	Cat# 18068015
NEB Gibson Assembly Master Mix	New England Biolabs	Cat# E2611
LR Clonase II	Invitrogen	Cat# 11791020
TOPO cloning kit	Invitrogen	Cat# K240020SP
Low Viscosity (Spurr's) Resin Kit	Electron Microscopy Sciences	Cat# 14300
Experimental Models: Organisms/Strains		
<i>Arabidopsis thaliana</i> : Col-0 wild type	Widely distributed	N/A
Arabidopsis: <i>7tm1-1</i>	Arabidopsis Biological Resource Center	SAIL_701_G12 in At5g18520
Arabidopsis: <i>7tm1-2</i>	Arabidopsis Biological Resource Center	Salk_134021 in At5g18520
Arabidopsis: <i>7tm2-3</i>	Arabidopsis Biological Resource Center	Sail_70_B11 in At3g09570
Arabidopsis: <i>7tm3-1</i>	Arabidopsis Biological Resource Center	Salk_062478 in At5g02630

REAGENT or RESOURCE	SOURCE	IDENTIFIER
Arabidopsis: <i>7tm4-1</i>	Arabidopsis Biological Resource Center	Sail_1_H08 in At5g42090
Arabidopsis: <i>7tm5-1</i>	Arabidopsis Biological Resource Center	Salk_044297 in At2g01070
Arabidopsis: <i>gpa1-4</i>	Jones et al., 2003	Salk_001846
Arabidopsis: <i>agb1-2</i>	Ullah et al., 2003	Salk_061896
Arabidopsis: <i>agg1-1c</i>	Trusov et al., 2007	FLAG_197F06 introgressed into Col-0
Arabidopsis: <i>agg2-1</i>	Trusov et al., 2007	SALK_010956
Arabidopsis: <i>agg3-1</i>	Chakravorty et al., 2011	SALK_018024
Arabidopsis: <i>agg1-1c agg2-1 agg3-1 (agg1/2/3)</i>	Thung et al., 2012	N/A
Arabidopsis: <i>prc1-1</i>	Fagard et al., 2000	N/A
Arabidopsis: <i>prc1-1 the1-1</i>	Hématy et al., 2007	N/A
Arabidopsis: CESA6pro:YFP-CESA6	Paredez et al., 2006	N/A
Arabidopsis: CESA3pro:GFP-CESA3	Desprez et al., 2007	N/A
Arabidopsis: CESA6pro:TdTom-CESA6	Sampathkumar et al., 2013	N/A
Arabidopsis: UBQ10pro:WAVE2-RFP	Geldner et al., 2009	N/A
Arabidopsis: UBQ10pro:WAVE7-RFP	Geldner et al., 2009	N/A
Arabidopsis: UBQ10pro:WAVE13-RFP	Geldner et al., 2009	N/A
Arabidopsis: UBQ10pro:WAVE18-RFP	Geldner et al., 2009	N/A
Arabidopsis: proVHAa1:VHAa1-mRFP	Dettmer et al., 2006	N/A
Arabidopsis: 35S:NAG-GFP	Grebe et al., 2003	N/A
Arabidopsis: 35S:GFP-LTI6b	Cutler et al., 2000	N/A
Arabidopsis: 35S: ST-RFP-2A-secGFP (ratiometric SecGFP)	Samalova et al., 2006	N/A
Arabidopsis: <i>7tm1-2</i> + 7TM1pro:7TM1-3xYFP	This paper, floral dip	N/A
Arabidopsis: <i>7tm1-2</i> + 7TM1pro:7TM1-mCherry	This paper, floral dip	N/A
Arabidopsis: <i>7tm5-1</i> + 35Spro:7TM5-CFP	This paper, floral dip	N/A
Arabidopsis: <i>gpa1-4</i> + UBQ10pro:GFP-GPA1	This paper, floral dip	N/A
Arabidopsis: <i>gpa1-4</i> + UBQ10pro:GPA1-GFP	This paper, floral dip	N/A
Arabidopsis: <i>agb1-2</i> + AGB1pro:AGB1-mCherry	This paper, floral dip	N/A
Arabidopsis: <i>agb1-2</i> + AGB1pro:mCherry-AGB1	This paper, floral dip	N/A
Arabidopsis: <i>agg1/2/3</i> + AGG1pro:mCherry-AGG1	This paper, floral dip	N/A
Arabidopsis: <i>agg1/2/3</i> + AGG2pro:mCherry-AGG2	This paper, floral dip	N/A
Arabidopsis: <i>agg1/2/3</i> + AGG3pro:mCherry-AGG3	This paper, floral dip	N/A
Arabidopsis: Col-0 + 7TM1pro:GUS	This paper, floral dip	N/A
Arabidopsis: Col-0 + 7TM5pro:GUS	This paper, floral dip	N/A
Arabidopsis: Other combinatorial lines generated via crossing	This paper	N/A
<i>Nicotiana benthamiana</i>	Widely distributed	N/A
Oligonucleotides		
See Table S2 for primers used for genotyping, cloning, and RT-PCR	This paper	N/A
Recombinant DNA		
7TM1pro:7TM1-3xYFP (genomic)	This paper	N/A

REAGENT or RESOURCE	SOURCE	IDENTIFIER
7TM1pro:7TM1-mCherry (genomic)	This paper	N/A
JATY76F23	Arabidopsis Biological Resource Center	JATY76F23
pEZR(K)-LNC-35Spro:7TM5-CFP (cDNA)	This paper	N/A
pUBN-eGFP-UBQ10pro:GFP-GPA1 (cDNA)	This paper	N/A
pUBC-eGFP-UBQ10pro:GPA1-GFP (cDNA)	This paper	N/A
pMDC99-AGB1pro:AGB1-mCherry (genomic)	This paper	N/A
pMDC99-AGB1pro:mCherry-AGB1 (genomic)	This paper	N/A
pMDC99-AGG1pro:mCherry-AGG1 (genomic)	This paper	N/A
pMDC99-AGG2pro:mCherry-AGG2 (genomic)	This paper	N/A
pMDC99-AGG3pro:mCherry-AGG3 (genomic)	This paper	N/A
pDOE-05	Gookin and Assmann, 2014	N/A
pDOE-10	Gookin and Assmann, 2014	N/A
pDOE-05 & pDOE-10 derivatives for BiFC assays as described in Method details	This paper	N/A
pCAMBIA3201-7TM1pro:GUS	This paper	N/A
pCAMBIA1305.1-7TM5pro:GUS	This paper	N/A
Software and Algorithms		
Fiji	Schindelin et al., 2012	<a href="https://imagej.net/Fiji">https://imagej.net/Fiji</a>
JaCOP plugin for Fiji	Bolte and Cordelières, 2006	<a href="https://imagej.net/JaCoP">https://imagej.net/JaCoP</a>
StackReg plugin for Fiji	Thévenaz et al., 1998	<a href="https://imagej.net/StackReg">https://imagej.net/StackReg</a>
ThunderSTORM plugin for Fiji	Ovesný et al., 2014	<a href="https://github.com/zitmen/thunderstorm">https://github.com/zitmen/thunderstorm</a>
FamNet	Ruprecht et al., 2016	<a href="http://aranet.mpimp-golm.mpg.de/famnet.html">http://aranet.mpimp-golm.mpg.de/famnet.html</a>
PlaNet	Ruprecht et al., 2016	<a href="http://aranet.mpimp-golm.mpg.de/index.html">http://aranet.mpimp-golm.mpg.de/index.html</a>
MEGA X	Kumar et al., 2018	<a href="https://www.megasoftware.net/">https://www.megasoftware.net/</a>
BoxPlotR	Spitzer et al., 2014	<a href="http://shiny.chemgrid.org/boxplotr/">http://shiny.chemgrid.org/boxplotr/</a>